Atorvastatin-loaded emulsomes foam as a topical antifungal formulation

Alaa S. Eita, Amna M.A. Makky, Asem Anter, Islam A. Khalil

PII: S2590-1567(22)00031-7

DOI: https://doi.org/10.1016/j.ijpx.2022.100140

Reference: IJPX 100140

To appear in:

Received date: 12 October 2022

Revised date: 10 November 2022

Accepted date: 19 November 2022

Please cite this article as: A.S. Eita, A.M.A. Makky, A. Anter, et al., Atorvastatin-loaded emulsomes foam as a topical antifungal formulation, (2022), https://doi.org/10.1016/j.ijpx.2022.100140

Atorvastatin-loaded emulsomes foam as a topical antifungal formulation

Alaa S. Eita [a,*], Amna MA Makky [b], Asem Anter [c], Islam A. Khalil [a]

[a] Department of Pharmaceutics, College of Pharmaceutical Sciences and Drug Manufacturing, Misr University for Science and Technology (MUST), 6th of October, Giza 12582, Egypt.
[b] Department of Pharmaceutics and Industrial Pharmacy, Faculty of Pharmacy, Cairo University, Cairo, Egypt.
[c] Microbiology Unit, Drug Factory, College of Pharmaceutical Sciences and Drug Manufacturing, Misr University for Science and Technology (MUST), 6th of October, Giza 12582, Egypt.

*Corresponding Author, email: alaa.eita@must.edu.eg

Corresponding Author:

Alaa S. Eita,

E-mail: alaa.eita@must.edu.eg

Address: Department of Pharmaceutics,

College of Pharmacy and Drug Manufacturing,

Misr University for Science and Technology,

6th of October City 12582, Giza, Egypt

Abstract

Dermal fungal infection faces many challenges, especially for immunocompromised patients. Recently, the repositioning of atorvastatin (ATO) as a promising anti-mycoses therapy is used to overcome some issues of conventional therapeutic agents such as microbial resistance. The goal of this study was to develop a suitable formula for dermal fungal infection. Wherefore, ATO was entrapped into emulsomes and then incorporated in a foam system for topical convenient application. The D-optimal design was used for the optimization of ATO-emulsome and foam to achieve suitable responses. Regarding emulsomes, cholesterol weight and sonication time were independent variables that impact emulsome size, polydispersity index, surface charge, and entrapment efficiency. The optimum formula showed a size of 359.4 ± 8.97 nm, PDI of 0.4752 ± 0.012, a zeta potential of -21.27 ± 0.53 mV, and a drug entrapment of 95 ± 2.38%. Transmission electron microscope and Fourier-transform infrared spectroscopy (FT-IR) proved the assembly of ATO-emulsome. Foam composition was optimized to achieve good expansion, stability, and viscosity using a surfactant triple mixture and hydroxypropyl methylcellulose. The selected ATO-emulsome foam which consisted of 1% HPMC, 1.49% SDS, and 4% pluronic showed prolonged drug release. Efficient permeation through skin layers was asserted by using a confocal laser scanning microscope. Moreover, the homogenous distribution of the foam bubbles upholds stability and conserves the system from rapid collapse. The antifungal activity was confirmed by an *in-vitro* and *in-vivo* microbiology study beside *in-vivo* biocompatibility. In conclusion, ATO-emulsome and incorporation in foam have demonstrated good antifungal activity which presented a unique aspect for potential clinical applications.

Keywords: Atorvastatin, Emulsomes, Foam, repurposing, fungal infection, topical

1. Introduction

Mycoses infection is one of the important challenges facing healthcare providers globally. Recent statics announced that at least 1.5 million deaths by mycoses infections are recorded worldwide yearly (Rayens and Norris, 2022). Superficial mycosis reported high resistance to conventional antifungal drugs due to widespread recurrent use, especially after the recent elevation in the immunocompromised patient population (Gupta and Venkataraman, 2022). Alongside resistance issues, the skin barrier is an obvious obstacle for topically applied therapy which preferred advanced formulation for optimum permeation (Sousa et al., 2020). Wherefore, continuous studies are conducted to reach solvation for those therapeutic issues.

Repositioning or repurposing established a promising useful method in therapeutic fields as an alternative concept in the pharmaceutical industry. This alternative strategy is supposed to highlight a new pharmacological indication for previously FDA-approved drugs (Sultana et al., 2020). Pre-approvement stages of drug discovery are highly laborious, costly, and time-consuming as they can spend 12-15 years, wherefore, repurposing is a savior and safe strategy for specific pharmaceutical and clinical needs (Hughes et al., 2011). Different therapeutic research regarding cardiology, oncology, and mycology resort to the repositioning strategy to solve different issues of known therapies such as side effects and multi-drug resistances (Peyclit et al., 2021). For instance, Tavakkoli et al. discussed the antifungal activity of statins against a wide range of fungus species (Tavakkoli et al., 2020).

Statins are well known cholesterol-lowering drug category that declined sterol biosynthesis by inhibiting the hydroxy-methyl-glutaryl coenzyme A (HMG-CoA) reductase (Matusewicz et al., 2015). Regarding different health conditions, statin revealed new potential therapeutic activities such as anti-inflammatory activity reported by Bradbury et al., an anticancer activity discussed by Hassanabad, and newly recognized antifungal activity (Bradbury et al., 2018; Hassanabad, 2019). Cabral et al. discussed the antifungal mechanism and refer it to the ability of statins to suppress the fungal reductase enzyme (HMG-CoA) leading to declining in the ergosterol level followed by fungal growth suppression (Cabral et al., 2013). Atorvastatin (ATO) is one of the statins reported with antimycotic activity on different fungus strains relying on previous microbiology studies (Ajdidi et al., 2020; Mahmoud et al., 2021a) Furthermore, previous work upholds the atorvastatin activity in animal models by formulating an emulgel to treat oral and vulvovaginal candidiasis (de Oliveira Neto et al., 2021). Using ATO with this new therapeutic field as an antifungal agent can overcome the drug resistance issue of conventional drugs. ATO dermal application preferred incorporation in nanocarriers system to ameliorate skin permeation and achieve higher efficacy without drug chemical alteration (Shahraeini et al., 2020).

Emulsomes (EMLs) are lipoidal nanovesicles that established favorable carriers for loading lipophilic drugs as they consist of a phospholipid outer layer with an inner lipidic core (El-Zaafarany et al., 2018). EMLs distinctive features uphold its utilization over other vesicles as it remarked with good stability, lower toxicity, and showed improvement in drug efficacy with a prolonged release profile (Fahmy et al., 2020). Furthermore, EMLs enhanced drug permeation and localization in skin layers and encourage depot action with elevation in therapeutic efficacy (R. Gupta et al., 2014). Noticeably, nanoparticle preparations for dermal administration preferred pre-loading in available topical formulations such as cream, gel, ointment, or lotion (Kurowska et al., 2019).

Foams were recently nominated as preferred vehicles for skin therapy in comparison with other conventional formulations. Foam advantages may refer to the ease of application, and the simple way of spreading with rubbing minimization preferable in contact with inflamed or sensitive skin, which leads to patient acceptance (Zhao et al., 2010b). Liquid foam formula is a dispersion of gas bubbles in a liquid phase containing surfactants that act as foaming agents with different additives as stabilizers and solvents in addition to the active ingredients (Parsa et al., 2019). Two methods are used to prepare the foam system as reported by Farkas et al., either by gas-supersaturation to yield an aerosol foam, or by simple mechanical shaking for a liquid solution that induces foaming posteriorly by using a non-propellant pump device (Farkas et al., 2019).

This study intends to highlight atorvastatin (ATO) antifungal activity relied on entrapping the drug in emulsome (EML) vesicles followed by loading it in a foam system to facilitate dermal application. The D-optimal design was employed to individually develop and optimize ATO-EMLs and blank foam systems for picking the optimum loading formulation. Several features were investigated regarding emulsomes and foams to insure system suitability and stability. Furthermore, *in-vitro* microbiology and *in-vivo* studies were conducted to prove drug activity and therapeutic efficacy. The study design is summarized in **Scheme 1**.

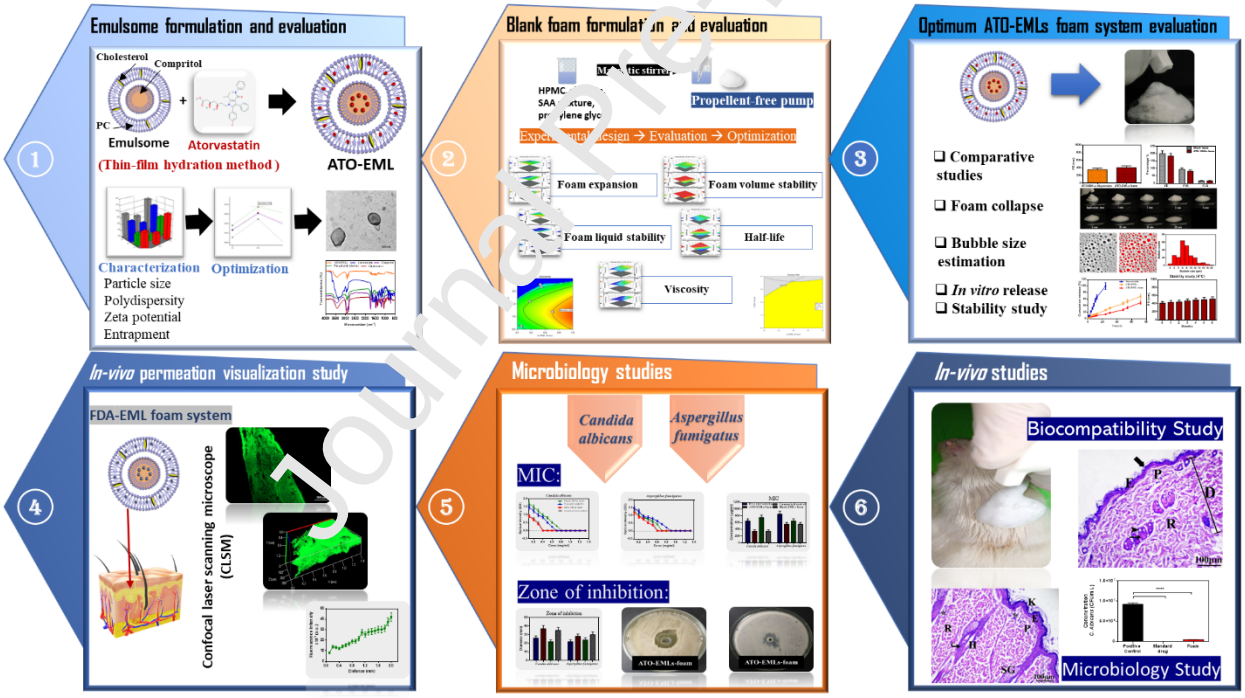

Scheme 1. Study design**:** *Phase 1* depicted the formulation and evaluation of atorvastatin-loaded emulsome (ATO-EMLs), *Phase 2* represents formulation and evaluation of blank foam systems, *Phase 3* shows further characterization of optimized ATO-EMLs foam system, *Phase 4* demonstrates skin tissue permeation by in-vivo visualization study using the confocal laser scanning microscope, *Phase 5* represents the microbiology studies of atorvastatin against C.albicans and A.fumigatus, *Phase 6* revealed the in-vivo studies.

2. Materials and Methods

2.1. Materials

Atorvastatin calcium was a kind gift from EIPICO, Egypt. Compritol 888 ATO was kindly gifted from Gatteffose, France. Soya phosphatidylcholine, cholesterol, sodium dodecyl sulfate (SDS), Pluronic f127, hydroxypropyl methylcellulose (HPMC), and cellulose membrane (Molecular weight cut off: 12,000), were purchased from Sigma-Aldrich (St. Loius, MO, U.S.A.). Propylene Glycol, tween 20, and buffer phosphate salts were purchased from El- Nasr Pharmaceutical Co. (Cairo, Egypt). All other used Chemicals were of analytical grade.

2.2. Emulsome formulation

2.2.1. Preparation of atorvastatin-loaded emulsome

As per the reported method (Zakaria et al., 2022), a thin film hydration technique was used for drug-emulsome incorporation with a slight alteration. Therefore, several atorvastatin-loaded emulsome (ATO-EMLs) formulae were prepared. A 90 mg Phosphatidylcholine (PC), 45 mg compritol, and variable cholesterol amounts were solubilized in a mixture of chloroform/methanol (2:1, v/v) and then mixed with 100 mg atorvastatin which was previously solubilized in a sufficient methanol amount. The mixture is exposed to reduced pressure until complete solvent evaporation by using a rotary evaporator. Subsequently, the residual film was hydrated with 15 ml of deionized water with gentle agitation for one hour at ambient temperature. The resulting formula was first subjected to bath sonication for one minute and then to probe sonication for different time intervals (750W, 20 kHz, and 55% amplitude) according to the employed design.

2.2.2. Experimental design of emulsome

Response surface methodology (RSM) established a considerable method for studies that are controlled by multivariate variables as implied by the wide utilization of Box–Behnken and central composite designs in scientific research (Habib et al., 2022). In this study, a D-optimal experimental design was utilized for ATO-EML formulae using Design-Expert® software (Stat-Ease Inc., Minneapolis, MN, USA) for studying multiple factors. The independent variables were cholesterol weight (mg, X_1), and probe sonication time (min, X_2), while particle size (nm, Y_1), polydispersity index (Y_2), Zeta potential (mV, Y_3), and entrapment efficiency (%, Y_4) were evaluated responses as shown in **Table 1**. Depending on the combination of different variables' levels, 17 experimental runs were generated by the software (Table 1 in supplementary file). Optimization suggestions rely on specific variable selections that lead to the most desirable formula with the lowest PS and PDI and the highest ZP and EE values.

Table 1: Variables and evaluated responses used in a D-optimal design for preparing and optimizing ATO-EMLs.

Independent variables	Levels			
X_1: Cholesterol weight (mg)	(-1) 4.5	(0) 22.5		(1) 45
X_2: Probe sonication time (min)	(-2) 12	(-1) 15	(1) 24	(2) 30
Evaluated responses	**Desirability constraints**			
Y_1: Particle size (nm)	Minimize			
Y_2: Polydispersity index	Minimize			
Y_3: Zeta potential (absolute value) (mV)	Maximize			
Y_4: Entrapment efficiency (%)	Maximize			

2.2.3. Evaluation of atorvastatin-loaded emulsome

2.2.3.1. Dynamic light scattering

For determining particle size (PS), polydispersity index (PDI), and zeta potential (ZP), the dynamic light scattering (DLS) technique was used at 25°C using Zetasizer (Malvern Instruments, Malvern, UK). Deionized water was used to dilute the emulsome dispersion 100-fold to reach a very slight hazy solution as the concentrated sample caused inaccurate measurements due to multiple scattering or viscosity effects. The diluted sample was added to the DLS disposable Folded Capillary cell (DTS1070) and thereafter, the mean, and standard deviation were computed in triplicate for all measurements (Abdellatif et al., 2020).

2.2.3.2. Entrapment and Loading efficiency

Drug entrapment efficiency or the amount of drug entrapped in the ATO-EML system was measured through an indirect method. One milliliter of the dispersion equivalent to 6.7 mg ATO was separated using a cooling centrifuge (Sigma 3 K 30, Germany) at 20000 rpm for 1 hour at 4°C. The unentrapped drug in the supernatant was removed and collected, while pellet residue was washed twice with deionized water and then recentrifuged for 1 hour to recollect the supernatant, as per the reported method (Varshosaz et al., 2019) with a slight alteration. The combined supernatant was analyzed using a UV–Vis spectrophotometer at 238.6 nm (Shimadzu UV 1650 Spectrophotometer, Japan). EE% was calculated in triplicate using the subsequent equation:

$$EE\% = \frac{T_{ATO} - U_{ATO}}{T_{ATO}} \times 100 \qquad \textbf{(Eq.1)}$$

T_{ATO} and U_{ATO} denote the total atorvastatin and unentrapped atorvastatin in the supernatant.

Drug loading was calculated in triplicate for optimum formula using the subsequent equation(Mahdi et al., 2021):

$$DL\% = \frac{T_{ATO} - U_{ATO}}{Weight\ of\ ATO-EMLs\ vesicle} \times 100 \qquad \textbf{(Eq.2)}$$

2.2.4. Characterization of optimized emulsome formula

2.2.4.1. Vesicle morphology

ATO-EMLs morphological study was assessed using a transmission electron microscope (TEM; CM12; Philips, USA). The optimized formula resulting from the experimental design was investigated to visualize the vesicle structure of the system. The sample was stained with an aqueous solution of 1.5% negative stain (phosphotungstic acid) and dried on a grid of carbon before being imaged (Albash et al., 2020).

2.2.4.2. Fourier transform infrared spectroscopy

Inspecting free ATO, PC, Cholesterol, Compritol, and optimized formula using Fourier transform infrared spectroscopy (FTIR) (Shimadzu IR- Affinity-1, Japan) was conducted. Scanning was applied in the range of 399-4000 cm^{-1} with a resolution of 4 cm^{-1} at ambient temperature with a speed of 2 mm/s (Zhao et al., 2015).

2.3. Foam formulation

2.3.1. preparation of foam system

Non- propellant foam formulation (NPF) was prepared as per the reported method (Kurowska et al., 2019), with slight modifications. Firstly, specific hydroxypropyl methylcellulose (HPMC) weight was levigated with 0.5% (w/v) propylene glycol (PG) and 1.5% (w/v) glycerin as a stabilizer (PG and glycerin amounts were determined previously upon experimental preliminary studies of foam physical stability with different ratio). Thereafter, different surfactant types and amounts depending on an establishing design were added to the HPMC blend and mixed with 15 ml of deionized water to prepare blank foam systems. The formulated mixtures were stirred on a magnetic stirrer (model MSH-20D, GmbH, Germany) for one hour at 1500 rpm. The propellent-free pump was used for foam formation from the aqueous solution at the time of investigation or application.

2.3.2. Experimental design of foam

Foam formulae were prepared according to a D-optimal design performed using Design-Expert® to assess the influence of foam specification at different compositions. The independent variables were concentration of HPMC (%, X_1), sodium dodecyl sulfate (SDS) (%, X_2), tween 20 (%, X_3), and pluronic (%, X_4). Otherwise, foam expansion (%, Y_1), foam volume stability (%, Y_2), foam liquid stability (%, Y_3), foam half-life (min, Y_4), and viscosity (cP, Y_5) were evaluated responses as shown in **Table 2**. Depending on the combination of different variables' levels, 24 experimental runs were established. Optimized formula with maximum desirability was selected upon evaluating all responses and estimating variables that retain the highest foam expansion (FE), foam volume stability (FVS), foam half-life, and viscosity, in addition to the lowest foam liquid stability (FLS).

Table 2: D-optimal design variables and evaluated responses for foam formulation.

	Levels	
	Low	**High**
X_1: HPMC concentration (%)	0.5	1
X_2: SDS concentration (%)	0	4
X_3: Tween 20 concentration (%)	0	4
X_4: Pluronic concentration (%)	0	4
Evaluated responses	**Desirability constraints**	
Y_1: Foam expansion (FE) (%)	Maximize	
Y_2: Foam volume stability (FVS) (%)	Maximize	
Y_3: Foam liquid stability (FLS) (%)	Minimize	
Y_4: Half-life (min)	Maximize	
Y_5: Viscosity (cP)	Maximize /In Range	

2.3.3. Foam evaluation

2.3.3.1. Foam calculated parameters

Different calculated parameters are employed in foam evaluation as they can help in a comparative study of different foam compositions or estimate foamability and stability attributes. The cylinder method is the way used in parameter measurements as reported previously (Arzhavitina and Steckel, 2010a). A specific volume of foam solution was used in foam production and visualized after 30 min. The initial volume of the solution and the produced foam volume were recorded, in addition to foam and drain volume after the studied time interval. Foam production in this study was done by homogenizing the sample volume (3 ml) in a falcon tube as the per reported method (Parsa et al., 2019; Zhang et al., 2014), which is more able to reduce foam formation variability between investigated formulae. Foam expansion (FE), foam volume stability (FVS), and foam liquid stability (FLS) were the calculating parameters according to shown equation (3-5).

Foam expansion (FE):

$$FE\% = \frac{Vfm - Vft}{Vft} \times 100 \qquad \textbf{(Eq.3)}$$

While (*Vfm) and (Vft)* are the resulting foam volume and the initial solution volume in milliliters, respectively.

Foam volume stability (FVS):

$$FVS\% = \frac{Vfm/30min}{Vft} \times 100 \qquad \textbf{(Eq.4)}$$

While (*Vfm*/30 min) is the foam volume in milliliters after 30 minutes.

Foam liquid stability (FLS):

$$FLS\% = \frac{Vl/30min}{Vft} \times 100 \qquad \textbf{(Eq.5)}$$

While (*Vl*/30 min) is the drained volume in milliliters after 30 minutes.

2.3.3.2. Foam half-life

Foam stability can be determined by foam half-life, which is the time required to reach half of its initial volume after foam production. A higher half-life time indicates preferred stability (Bai et al., 2019). As discussed previously, the homogenizer was used for foam formation (Parsa et al., 2019).

2.3.3.3. Viscosity

The viscosity of the liquid formulation establishes a critical role in pump-producing foam and foamability. By using Brookfield DV3T Viscometer (Brookfield Engineering Laboratories, Inc., Middleboro, MA) viscosity was measured in triplicate at a temperature of 25°C± 2°C and 250 rpm (Derikvand and Riazi, 2016).

2.4. Characterization of optimum ATO-EMLs foam formulation

2.4.1. Comparative study with ATO-EMLs and blank foam

PS and PDI of ATO-EMLs incorporated in the foam system were evaluated to ensure foam availability as a carrier system for effective topical application. In addition, foam calculated parameters and half-life were remeasured to reflect any changes in the characteristic features of the optimized foam formulation.

2.4.2. Foam collapse

Foam collapsing capability was estimating foam acting on the application site upon actuating one pumping from the non-propellant pump device onto a glass surface. Photos of actuating foam from the side view were taken at different time intervals for collapsing process documentation and height measurements. Moreover, the reduction of the foam height original value to less than 10% determined the collapse time (Farkas et al., 2021).

2.4.3. Bubble size estimation

Bubble size and distribution were measured by using ImageJ (U. S. NIH, Maryland, USA). Image analysis was done on a foam picture taken after the actuation occurred on a glass surface. Photograph adjustment was conducted using the software and the size distribution histogram was illustrated versus globule mean bubble size (μm) (Farkas et al., 2019).

2.4.4. *In-vitro* release study

The release study was conducted by utilizing a diffusion cell to determine the release profile of free atorvastatin, the best ATO-EML nanovesicle, and the optimum ATO-EML foam system. In

a receiver chamber, a diffusion media consisting of 100 ml PBS (PH:5.5) containing 10% propylene glycol was kept under adjusting temperature maintained at 32 ± 0.5°C with continuous stirring at 100 rpm. Propylene glycol is used to maintain sink conditions as noticed by Mahmoud et al. while using propylene glycol in the media of ATO released from dermal transfersomes (Mahmoud et al., 2017). Emulsomal dispersion of one and a half milliliters amounting to 10 mg ATO was placed in the donor compartment of the diffusion cell with a surface area equal to 5 cm^2. Samples from the receiver compartment were withdrawn at predetermined time intervals to calculate the drug concentration estimated by UV/visible spectrophotometer, instantaneously the compartment was compensated with equal volumes of fresh medium.

The release study was kinetically analyzed by subjecting the resulting data to different models such as zero order, first order, second order, Higuchi model, Weibull model, and Hixson–Crowell model, etc., looking for the best fitting one with a higher correlation coefficient (R^2) using (KinetDS) software (Mendyk et al., 2012). Interpretation of data based on Costa and Sousa Lobo, and Zhang et al. (Costa and Sousa Lobo, 2001; Zhang et al., 2010).

2.4.5. Stability study

Optimized loaded foam formulation was stored in a glass vial at 4 ± 1°C to determine system stability by tracking loading nanoparticle-specific features for 6 months. Physical appearance, PS, PDI, and ZP were examined as an indication of the physicochemical stability of the ATO-EML foam solution. Furthermore, foam producibility was evaluated to ensure system applicability. Measurements were taken immediately in triplicate after the system was prepared and during the sample monthly investigation.

2.5. *In-vivo* permeation visualization study

As deep penetration is expected from loaded foam formulation and is preferred for better application. The depth of the drug-loaded system was simulated by loading fluorescent dye instead of the drug to support system tracking. Subsequently, a visualization using confocal laser scanning microscopy (CLSM) was applied, as targeting deep layers of the skin was in demand (Mahmood et al., 2014).

2.5.1. Preparation of FDA-loaded foam system

As mentioned previously, the thin film hydration technique was used for emulsome preparation. Fluorescein Diacetate (FDA) was incorporated instead of ATO, and thereafter FDA-EML was loaded into the optimized foam system.

2.5.2. Skin preparation

The Study of the *in vivo* permeation was conducted under the ethical committee approval of the Department of Pharmacy, Cairo University (Protocol serial number PI 2850). An albino rat was prepared by marking and shaving a specific zone on the dorsal area measuring about 2 cm^2. An FDA-loaded foam system was applied to the specified area and stayed for 24h. Later on, after application, the rat was sacrificed by cervical dislocation method, and skin tissue of the application area was excised and kept at -20°C until CLSM observation as previously reported

by Kassem et al. while utilizing *in vivo* visualization strategy using CLSM for niosomal hydrogel on rat skin (Kassem et al., 2017).

2.5.3. Confocal laser scanning microscopy study

A longitudinal section of the skin tissue was examined and visualized using a microscope (LSM 710; Carl Zeiss, Oberkochen, Germany). The excitation wavelength of the FDA is 488 nm, while the emission wavelength is 530 nm. The investigation provided qualitative and quantitative evidence of the system permeation pattern considering skin thickness. Scanning occurred optically from the surface of 0 µm to 300 µm at 15 µm increments. Permeation of the foam system in skin layers was reflected by structuring a 3D plot using Z-stack mode (Abdellatif et al., 2017).

2.6. *In-vitro* microbiology study

2.6.1. Fungal strains

Standard strains of *Candida albicans* and *Aspergillus fumigatus* employed in this study were obtained from the culture collection unit at the Regional Center for Mycology and Biotechnology (Al Azhar University). On sabouraud dextrose agar (SDA) media each strain was sub-cultured and incubated for 24 h at 37° C to obtain the required inoculums for the study.

2.6.2. Inoculum preparation

From 24h old culture about two or three colonies were used as the inoculum following suspension in 10 ml of 0.85% sodium chloride solution, which was autoclaved. The turbidity was adjusted to 0.5 McFarland standard units (i.e., 1.5×10^8 CFU/ml) (Alyousef, 2021).

2.6.3. Micro-Well Dilution Method

The microdilution method determined the minimum inhibitory concentration (MIC) values of evaluated samples against C.albicans and A.fumigatus (Zhang et al., 2020). The assay was performed on the free ATO, blank EML-foam, and ATO-EML foam system. Samples pre-exposed to two-fold serial dilutions to achieve concentrations from 1.32 to 0.1 mg/ml and then inoculated in a microplate containing broth media. The culture plates were incubated at 37°C for 24 h. Sabouraud broth only and broth with microorganisms were used as a negative and positive control, respectively to determine medium sterility and inoculum viability. Moreover, Fungistate® gel as a standard commercial control was assessed. The optical density was measured in triplicate for MIC determination of investigated formulae.

2.6.4. Well diffusion method

Antifungal activity was conducted using a well diffusion method for assessment of free ATO, blank EML foam, and ATO-EML foam system on C.albicans and A.fumigatus strains. Commercial Fungistate® gel was used as positive control while saline was used as a negative control. About 15-20 ml of the prepared SDA media was poured and spread homogeneously in sterile Petri dishes, then remained for half an hour to solidify. Subsequently, 0.2 ml of the inoculum was spread on an agar plate, and discarded the excess via a drain. The plates were then

incubated for 10 min at ambient temperature. Thereafter, a 4 mm ditch was made on each plate, and 50-100 microliters of the diluted formulae were transferred into wells. The plates were incubated for 24 h at 37° C, and then a zone of inhibition was measured in millimeters as triplicate for each sample (Senyiğit et al., 2014).

2.7. *In-vivo* studies

2.7.1. Biocompatibility Study

In-vivo biocompatibility study was conducted to evaluate the biocompatibility of ATO-EML foam. This study was carried out according to the guidelines approved by the ethical committee of the Department of Pharmacy, Cairo University (serial number of the protocol PI 2850). Two groups of Wistar albino rats (6 per group, male, 200–250 g, normal chow/ad Lib) were assigned to placebo foam and ATO-EML foam. The foam was applied on the dorsal side of the rats after shaving. For 3 weeks, the area of application was observed to assess any skin erythema, and rats were sacrificed after one and three weeks by the cervical dislocation method. The dorsal skin was collected for histopathological evaluation, where the skin samples were washed, fixed, dehydrated, and embedded in paraffin. Skin sections were collected (5-7 µm), deparaffinized, and stained by hematoxylin and eosin (H&E) (Suvarna et al., 2012).

2.7.2. Microbiological study

The antimicrobial activity of ATO-EML foam was tested using a dermal fungal infection rat model according to the guidelines approved by the ethical committee of the Department of Pharmacy, Cairo University (serial number of the protocol PI 2850). Three groups (6 per group, male, 200–250 g, normal chow/ad Lib) were assigned to the positive control (infection only), standard drug (Terbinafine HCl with a once-daily dose), ATO-EML foam (one dose (6.7mg/ml) every 3 days). For the induction of fungal infection, betamethasone (2 mg/kg body weight/day, 3 times for 3 days) was injected subcutaneously to suppress immunity. On day 4, 100µl of *Candida albicans* (ATCC 10231, 10^7 CFU/mL) was injected into dorsal skin after shaving (Abdellatif et al., 2017). After 3 days from fungal induction, the application of medicated foam was applied for 3 weeks. At the end of the study, rats were sacrificed by the cervical dislocation method. Skin samples were collected for histopathological and microbiological examination. For microbiological evaluation, homogenized skin samples were incubated in sabourad dextrose agar culture media (48h at 37°C) followed by colony count (CFU). Histopathological examination was conducted as previously mentioned in the skin irritation test.

2.8. Statical analysis of data

The student's t-test, one-way, and two-way analysis of variance (ANOVA) with Tukey's post hoc tests were applied to determine significant differences between inspected samples. A 0.05 settled as significance level, and (* $p < 0.05$, ** $p < 0.01$, *** $p < 0.001$ and **** $p < 0.0001$) supposed to be statistically significant. (Data analysis performed by prism 6 software)

3. Results and discussion

3.1. Experimental analysis of emulsome formulation

Design-Expert software was utilized to analyze data resulting from the design experimental trials (**Table 1 in supplementary data)** using analysis of variance (ANOVA). The effects of cholesterol weight and sonication time as independent variables on several responses were tracked by response surface methodology using a D-optimal design. ANOVA results were illustrated in **Table 3** for the 2FI model while lack of fit was insignificant for all responses.

Table 3: ANOVA results of the 2FI model for emulsome formulae optimal design responses.

Response	R^2	Adjusted R^2	Predicted R^2	Adequate precision	F-value	P-value	Significance
PS (nm)	0.9356	0.9063	0.8416	18.7644	31.96	< 0.0001	significant
PDI	0.9251	0.8911	0.8189	16.8398	27.18	< 0.0001	Significant
ZP (mV)	0.9099	0.8970	0.8651	17.1398	70.70	< 0.0001	Significant
EE (%)	0.7874	0.7570	0.6923	9.3983	25.92	< 0.0001	Significant

Abbreviations: PS, particle size; PDI, polydispersity index, ZP, zeta potential; EE, entrapment efficiency.

3.1.1. Variables impact on evaluated responses

3.1.1.1. Particle size and Polydispersity index

Variables affecting PS and PDI were widely assessed as both responses impact nanovesicle systems regarding stability, permeability, and clinical applicability (Danaei et al., 2018). Cholesterol weight (X_1) and sonication time (X_2) both significantly influenced PS and PDI (**Fig.1a-b**) as shown by the interaction plot in **Fig.1e-f**. Concerning the cholesterol effect, firstly by weight augmenting a reduction in PS and PDI was observed followed by elevation in the same responses with the highest cholesterol level as shown graphically in **Fig.1a-b** ($p < 0.0001$). Cholesterol can regulate membrane rigidity, fluidity, and stability but in consideration of dependent concentration as elevation may induce fusion and aggregation (Camilo et al., 2020). As previously discussed by Khan et al. during the evaluation of transfersomes vesicles, the incorporation of cholesterol in the vesicle system may cause an increment in PS and PDI as a result of increasing surface hydrophobicity which stimulates particle aggregation. In addition, growth in the lipid membrane thickness by 3 Å with the addition of cholesterol was observed while using X-ray diffraction (Khan et al., 2021).

Probe sonication time (X_2) effect gives rise to a significant change in PS ($p = 0.0002$) and PDI ($p = 0.0001$). A reduction in PS and PDI was determined with increasing sonication time up to 15 min, however, further time elevation led to a reverse effect as illustrated graphically by the interaction plot in **Fig.1e,f**. Probe sonication mechanical waves produce higher energy on dispersed particles leading to size minimization as mentioned by Fahmy et al. upon studying ultrasonication time as an independent variable on emulsome fabrication (Fahmy et al., 2020). While exposed nanoparticles to extended sonication time, small particles were stimulated to coalesce and form polydisperse and larger particles as suggested by Pradhan et al. upon assessing

the effect of sonication on nanoparticle dispersion (Pradhan et al., 2016). The effect of variables on Particle size and Polydispersity index was demonstrated by 3D plot in **Fig.1** and polynomial Equations (6-7):

$PS=800.70-28.84*X_1[-1]\ -213.30*\ X_1[0]\ -37.80*\ X_2[-1]\ -220.90*\ X_2[0]\ +61.08*\ X_2[1]$ **(Eq.6)**

$PDI\ =0.74+0.04*\ X_1[-1]\ -0.12*\ X_1[0]\ +0.019*\ X_2[-1]\ -0.13*\ X_2[0]\ -0.006*\ X_2[1]$ **(Eq.7)**

3.1.1.2. Zeta potential

ZP of the emulsome dispersion indicates the charge of the surface, and the higher values (regardless of the sign) established higher repulsive forces that minimize aggregation and induce vesicle stabilization (Awan et al., 2020). ZP values of formulated ATO-EMLs ranged from -17.62 to -26.13 mV (**Fig.1c**). The negative charge of the formulated EMLs could be ascribed to anionic phospholipids in the outer shell layer. Similar findings were reported by Aldawsari et al., El-Zaafarany et al., Zhou and Chen upon emulsome fabrication using phospholipids in different levels, as all prepared emulsome systems acquired negative zeta potential (Hibah M Aldawsari et al., 2021; El-Zaafarany et al., 2016; Zhou and Chen, 2015). Concerning X_1, by increasing cholesterol weight a significant elevation ($p < 0.0001$) in ZP (absolute value) was demonstrated in **Fig.1g**. Higher ZP owing to the hydrogen bonds between cholesterol and phospholipids, which lead to promotes electronegative atom as reported in Song et al, while studying sterols effect on vesicle system (Song et al., 2022). In contrast, sonication time (X2) remarked with insignificant impact as shown in **Fig.1g**. The effect of variables on the Zeta potential was illustrated by 3D plot in **Fig.1** and polynomial Equation (8):

$ZP = -21.54 +2.86*X_1[-1] +0.21*X_1[0]$ **(Eq.8)**

3.1.1.3. Entrapment efficiency

Drug loading in a lipidic vesicular system ameliorates biological availability and may control the release of the drug (Hibah M. Aldawsari et al., 2021). Upon studying the effect of cholesterol weight (X_1) and sonication time (X2) on EE **(Fig.1d,h)**, a significant change was recorded concerning cholesterol ($p < 0.0001$), otherwise sonication time showed no significant effect on this response.

All prepared formulae (**Table 1 in supplementary data)** showed higher entrapment efficiency (EE% > 85%) that could be explained by the highly lipidic structure of the emulsome core-shell system which constructs a favorable space for lipophilic drug loading as reported by Bolat et al.(Bolat et al., 2020). Moreover, the formulae with the highest cholesterol level acquired the higher drug-entrapped percent as the incorporation of cholesterol in the phospholipid shell causes a pronounced impact on the entrapment of drugs with lipidic nature (Sawant et al., 2016). Wherefore, the lipidic nature of atorvastatin assists entrapment efficiency. The effect of variables on the Entrapment efficiency was elucidated by 3D plot in **Fig.1** and polynomial Equation (9):

$EE =+94.03-3.29*X_1[-1]+1.30*X_1[0]$ **(Eq.9)**

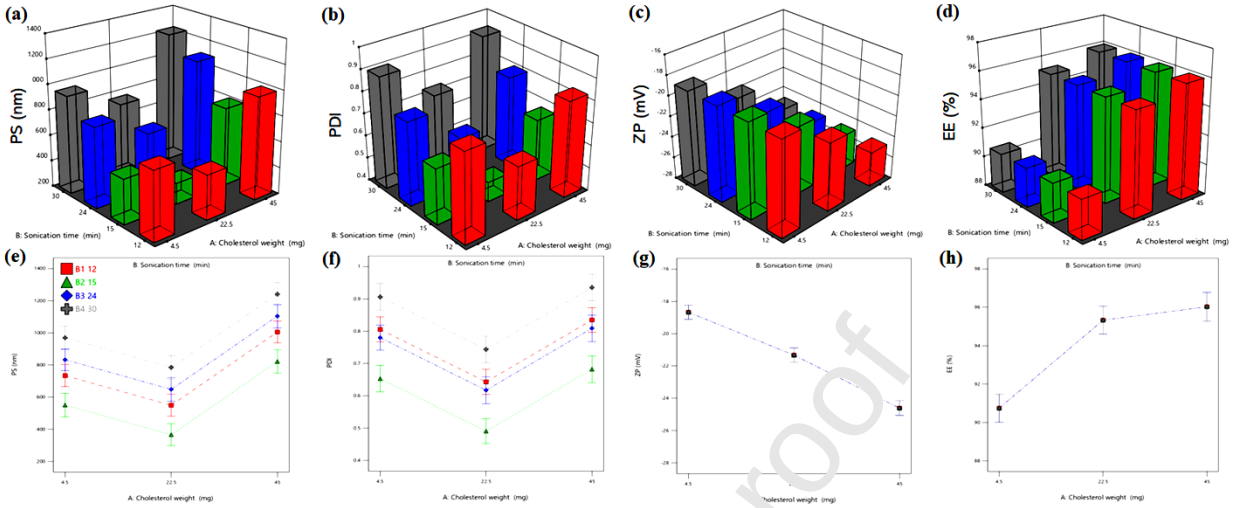

Fig.1. 3D plot of cholesterol weight and sonication time impact as independent variables on (a) Particle size (PS), (b) Polydispersity index (PDI), (c) Zeta potential (ZP), and (d) Entrapment efficiency (EE), **Graphically illustrated of variables interaction** upon studying (e) Particle size (PS), (f) Polydispersity index (PDI), (g) Zeta potential (ZP), and (h) Entrapment efficiency (EE);results represent the significant influence of cholesterol on all variables, otherwise, sonication time affect PS and PDI only.

3.1.2. Optimization of ATO-EMLs using D-optimal design

Design expert software was employed for optimum ATO-EMLs selection according to the desirability function. Optimization targets minimizing PS and PDI, while maximizing absolute ZP magnitude and EE. The suggested cholesterol weight of optimized formulae was 22.5 mg, in addition to the utilization of probe sonication for 15 minutes to fulfilled required attributes with the higher recorded desirability of 0.756 as shown in **Fig.2a**, E1 and E16 both include the required variables, E1 was selected for further investigation and showed vesicle particle size of 359.4 ± 8.97 nm, PDI of 0.4752 ± 0.012, a zeta potential of -21.27 ± 0.53 mV, and a drug entrapment of 95 ± 2.38%.The selected optimized formulation showed a drug loading of 37.6± 0.94%.

3.2. Characterization of selected emulsome formula

Further investigation was conducted on the selected ATO-EMLs formula which acquired the higher desirability with the minimum PS and PDI together with the maximum ZP (absolute) and EE values.

3.2.1. Vesicles morphology

The microscopic examination of the selected formula using TEM illustrated in **Fig.2b** appeared as a spherical nano vesicle with a smooth uniform surface. An outer shell of phospholipid with an inner core of compritol was remarked. As reported by Kamel et al. while using emulsome as a carrier for a natural anticancer compound, the TEM photograph showed a rounded shell layer with a dense inner lipid core in a nano-size revealed with no aggregation (Kamel et al., 2022). Our result reflects a similar emulsome morphology.

3.2.2. Fourier transforms infrared spectroscopy

FTIR established a suitable method for confirmation of drug entrapping in lipid vesicles as the disappearing of ATO characteristic peaks indicates efficient drug entrapment as discussed previously by Yadav et al. (Yadav et al., 2020). FTIR spectra of Atorvastatin, Cholesterol, PC, Compritol, and optimized ATO-EMLs formulation were shown in **Fig.2c**. The FTIR spectrum of pure ATO showed many distinctive peaks mainly at about 3606.5 cm^{-1} corresponding to non-hydrogen-bonded O-H, 3363.7 cm^{-1} to N-H stretching, 3257.35 cm^{-1} to O-H stretching, 2970.36 cm^{-1} to C-H stretching, 2920.2 cm^{-1} to C-H, aromatic, 1651.1 cm^{-1} to C=O stretching, 1577.75 cm^{-1} to N-H bending, 1508.31 cm^{-1} to C-N stretching, 1434.87 cm^{-1} to O-H bending, and 1381.2 cm^{-1} to C-O stretching linked to the carboxyl group as reported by da Silva et al. and Ghanem et al. (da Silva et al., 2016; Ghanem et al., 2021). Compritol and cholesterol acquired several bands with a characteristic broad band between 3600 cm^{-1} and 3200 cm^{-1} related to OH stretching (Aburahma and Badr-Eldin, 2014; U. Gupta et al., 2014). The disappearance of the mentioned ATO and core composition peaks confirmed emulsome fabrication with efficient loading.

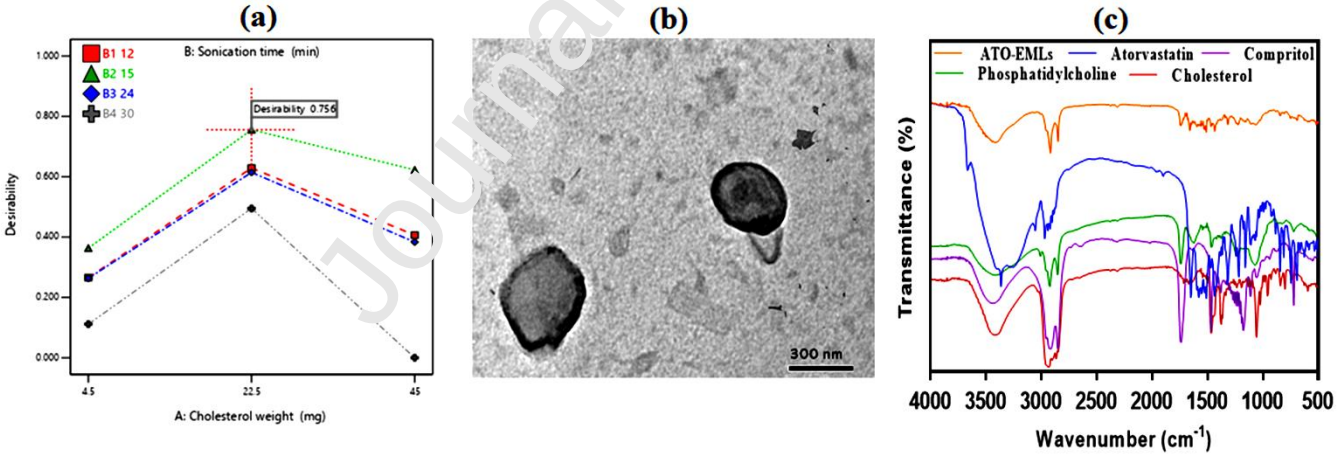

Fig.2. (a) **Interaction plot** showing independent variables desirability for selected ATO-EMLs optimum formula, **Further characterization on the optimum formula:** (b) TEM image of emulsome vesicle system; observed uniform spherical shape around 300 nm in size, (c) Fourier transforms infrared spectra for free atorvastatin, cholesterol, compritol, phosphatidylcholine, and optimum emulsome formula; prove vesicle formation and efficient drug loading.

3.3. Experimental analysis of blank foam preparations

As RSM established a suitable method to achieve an optimal suggestion relying on the relationship between multivariate factors and responses (Beg et al., 2019), several experimental trials (**Table 2 in supplementary data)** were generated and then analyzed using analysis of variance (ANOVA). Studying the effect of surfactants (SAA) (SDS, pluronic, tween 20) with different concentrations in addition to HPMC concentration regarding foam-specific features were tracked, and ANOVA results are shown in Table 4 while lack of fit was insignificant for all responses.

Table 4: ANOVA results of foam experimental trials.

Response	Model	R^2	Adjusted R^2	Predicted R^2	Adequate precision	F-value	P-value	Significance
FE (%)	Quadratic	0.9858	0.9638	0.7860	34.7602	44.79	< 0.0001	significant
FVS (%)	Quadratic	0.9791	0.9467	0.8797	22.4882	30.17	< 0.0001	Significant
FLS (%)	Quadratic	0.9737	0.9329	0.8513	20.0658	23.84	< 0.0001	Significant
Half-life (min)	2FI	0.8840	0.7948	0.6816	11.5361	9.91	0.0001	Significant
Viscosity (cP)	Quadratic	0.9969	0.9922	0.9568	47.9531	208.86	< 0.0001	Significant

Abbreviations: FE, foam expansion; FVS, foam volume stability; FLS, foam liquid stability.

3.3.1. Variables impact on foam evaluated responses

3.3.1.1. Foam calculated parameters

Higher FE indicates more foamable formula, while higher FVS refers to maximum foam stability. In addition, FLS relates to drain stability and shows a reverse relationship with foam stability (Arzhavitina and Steckel, 2010b; Farkas et al., 2019).Y. Wang et al. explained in a previous experimental study that a higher hydrophilic-lipophilic balance (HLB) value of surfactants observed higher foaming capacity with a more stable state due to increased SAA hydrophilicity which tends to reduction in gas-liquid interfacial tension (Y. Wang et al., 2017). As shown in **Fig.3a-i**, higher foam expansion remarked with higher SDS concentration as it related to the HLB value of the surfactants which are 40, 22, 16.7 for SDS, pluronic f127, and tween 20 respectively. Furthermore, higher concentrations of triplicate mixture enhance FVS and reduce FLS as depicted in **Fig.4a-i** and **Fig.5a-i**, respectively. Carey and Stubenrauch reported that the foamability of the SAA mixture does not exceed the remarked value of the single ionic SAA (SDS) formulation with the highest recorded foamability attribute, but it affects positively the foam volume stability (Carey and Stubenrauch, 2010).The effect of variables on the Foam expansion, Foam volume stability, and Foam liquid stability was elucidated by 3D plot in **Fig.3-5** and polynomial Equations (10-12):

$$FE = 102.81 - 7.08*X_1 - 74.13*X_2 - 46.73*X_3 - 27.97*X_4 - 23.81*X_1*X_2 + 10.49*X_1*X_3 + 34.87*X_1*X_4 - 59.36*X_2*X_3 - 43.93*X_2*X_4 - 27.36*X_3*X_4 + 15.97*(X_1)^2 - 38.45*(X_2)^2 - 22.99*(X_3)^2 - 4.21*(X_4)^2 \quad \textbf{(Eq.10)}$$

$$FVS = +96.21 + 6.05*X_1 + 22.32*X_2 + 31.71*X_3 + 28.13*X_4 - 2.04*X_1*X_2 + 1.01*X_1*X_3 - 2.08*X_1*X_4 + 23.38*X_2*X_3 + 22.67*X_2*X_4 + 18.34*X_3*X_4 + 0.024*(X_1)^2 - 7.15*(X_2)^2 + 17.99*(X_3)^2 + 2.56*(X_4)^2 \quad \textbf{(Eq.11)}$$

$$FLS = -0.0711 - 9.71*X_1 - 69.30*X_2 - 77.84*X_3 - 70.13*X_4 + 3.69*X_1*X_2 + 5.15*X_1*X_3 + 5.49*X_1*X_4 - 62.08*X_2*X_3 - 52.01*X_2*X_4 - 41.32*X_3*X_4 + 6.36*(X_1)^2 - 10.22*(X_2)^2 - 41.72*(X_3)^2 - 6.41*(X_4)^2 \quad \textbf{(Eq.12)}$$

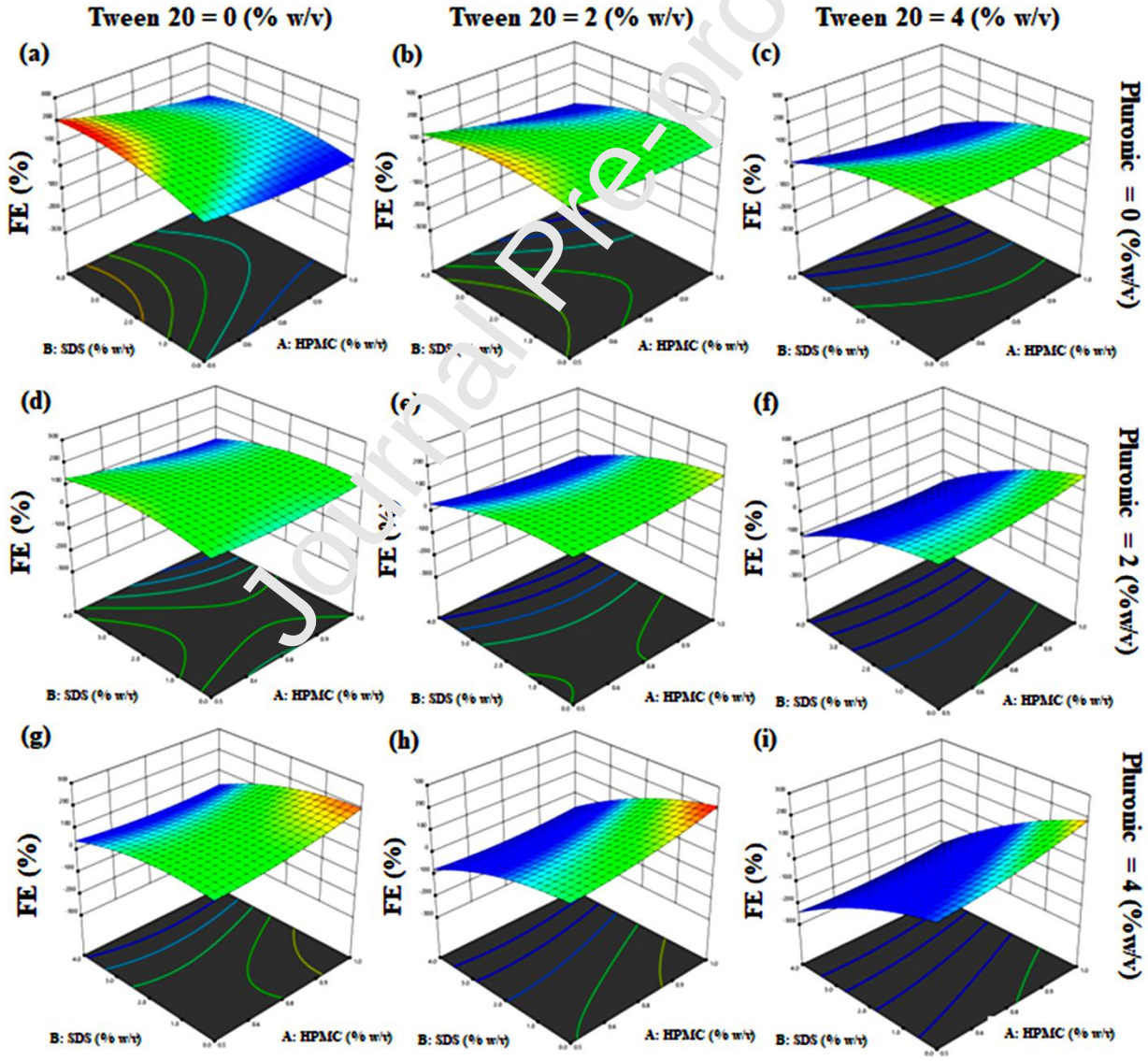

Fig.3. 3D plots of foam expansion (%) response corresponding to different variable levels; **pluronic low level:** 0% (w/v) with different concentration (% w/v) of Tween 20 (a) 0, (b) 2, (c) 4, **pluronic medium level:** 2% (w/v) with different concentration (% w/v) of Tween 20 (d) 0, (e) 2, (f) 4, **pluronic high level:** 4% (w/v) with different concentration (% w/v) of Tween 20 (g) 0, (h) 2, (i) 4. (Measured responses color change from blue to red indicate increase response value)

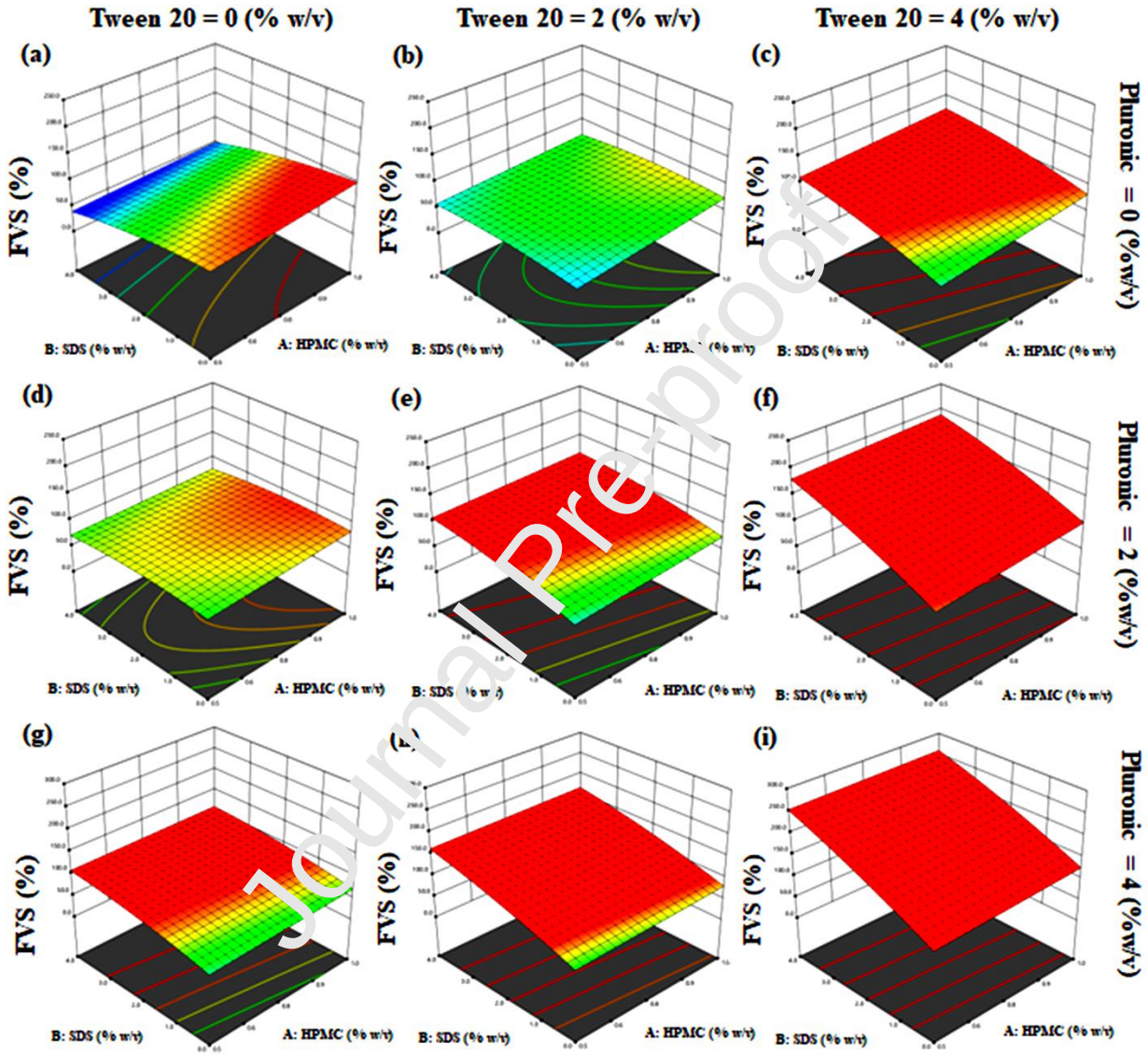

Fig.4. 3D plots of foam volume stability (%) response corresponding to different variable levels; **pluronic low level:** 0% (w/v) with different concentration (% w/v) of Tween 20 (a) 0, (b) 2, (c) 4, **pluronic medium level:** 2% (w/v) with different concentration (% w/v) of Tween 20 (d) 0, (e) 2, (f) 4, **pluronic high level:** 4% (w/v) with different concentration (% w/v) of Tween 20 (g) 0, (h) 2, (i) 4.

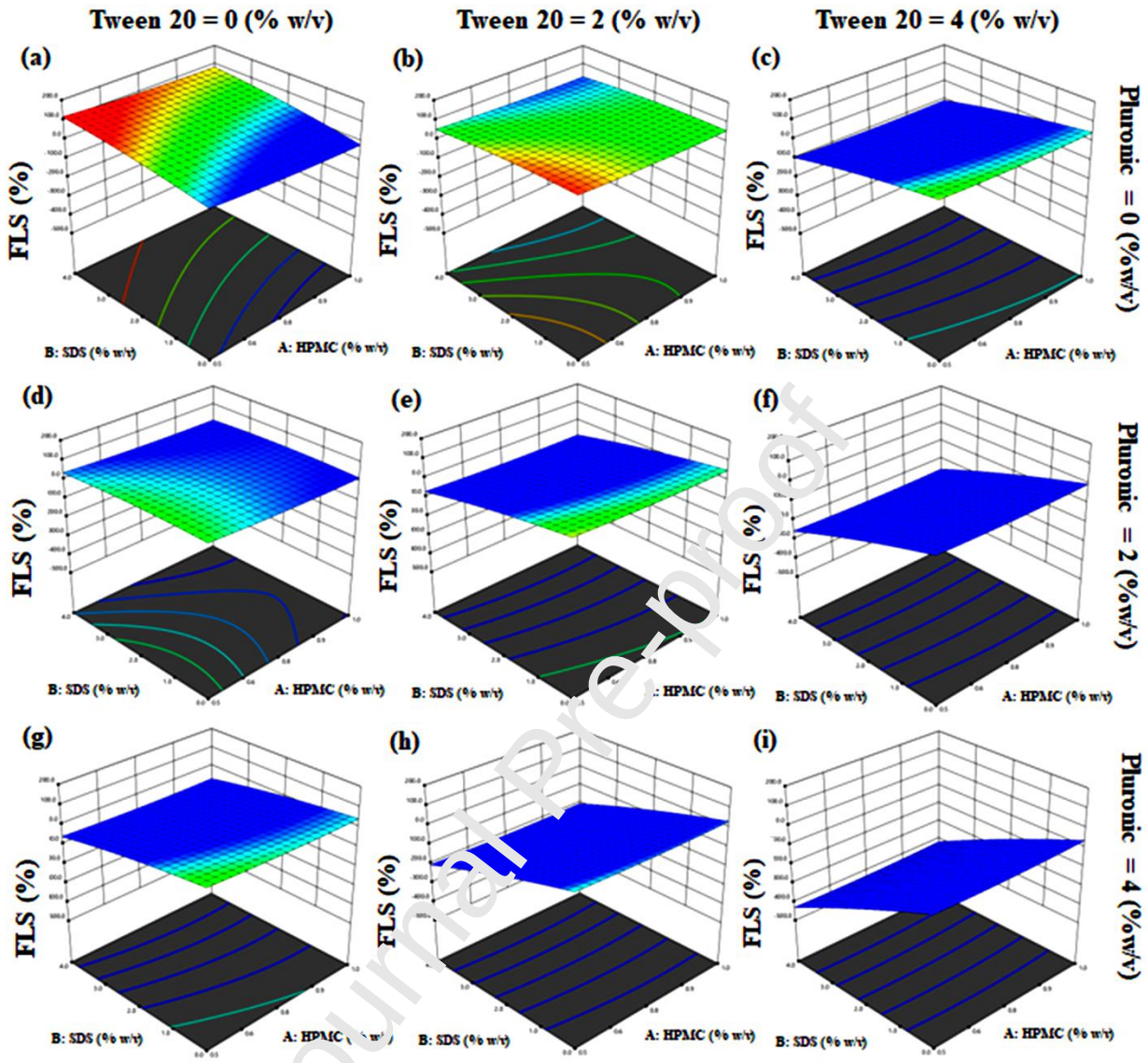

Fig.5. 3D plots of foam liquid stability (%) response corresponding to different variable levels; **pluronic low level:** 0% (w/v) with different concentration (% w/v) of Tween 20 (a) 0, (b) 2, (c) 4, **pluronic medium level:** 2% (w/v) with different concentration (% w/v) of Tween 20 (d) 0, (e) 2, (f) 4, **pluronic high level:** 4% (w/v) with different concentration (% w/v) of Tween 20 (g) 0, (h) 2, (i) 4.

3.3.1.2. Foam half-life

Measuring foam half-life should be conducted to determine foam efficiency by indicating foam stability (Derikvand and Riazi, 2016). As illustrated in **Fig.6a-i**, generally, by increasing surfactants concentration long half-life values were detected. Wang et al. upon studying the influence mechanism of foaming agents on stability, observed an increase in half-life with higher concentrations until reached a specific limit referred to as maximum stability concentration. An

explanation revealed to critical micelle concentration (CMC) states that exceeds CMC minimizing the surface tension and forming micelles with different shapes gradually until establishing a lamellar form with higher thermodynamically stable attributes (H. Wang et al., 2017). Furthermore, nonionic surfactants are supposed to produce favorable foam stability as shown with pluronic (Bera et al., 2013). In **Fig.6g,** the slight reduction occurs in half-life with the higher levels of Tween 20 alongside with pluronic may refer to the synergistic effect of both nonionic surfactants resulting in overpass maximum stability concentration. The effect of variables on the half life was illustrated by 3D plot in **Fig.6** and the polynomial Equation 13:

$$\text{Half life} = 100.09 + 28.66*X_1 + 38.78*X_2 - 21.48*X_3 + 26.31*X_4 + 10.72*X_1*X_2 + 15.44*X_1*X_3 + 13.00*X_1*X_4 + 2.08*X_2*X_3 + 44.03*X_2*X_4 - 38.69*X_3*X_4 \quad \textbf{(Eq.13)}$$

3.3.1.3. Viscosity

Viscosity is established a critical role in foam preparation as it influences both foamability and foam stability. A lower viscosity support foam generation while augmenting values uphold stability lifetime (Bureiko et al., 2015). Wherefore, Gennari et al. noticed that a viscosity-modifying agent is required to create foam with optimum properties, otherwise, the concentration should not exceed 2% to be capable of foam fabrication (Gennari et al., 2019). As depicted in **Fig.7a-i**, the highest HPMC concentration (1%) showed the maximum viscosity in all cases. Moreover, Surfactants revealed higher viscosity individually while in mixtures and higher SAA concentrations a reverse effect was recorded as shown in **Fig.7i**, with the lowest viscosity remarked with higher SAA levels. Reduction in viscosity values can be explained as reported by Eftekhari and Farajzadeh, who noticed that stronger foam production prefers lower SAA concentration, while with an augmentation, higher micelles concentration results which may be captured in the thinning process (Eftekhari and Farajzadeh, 2017). The effect of variables on the viscosity was elucidated by 3D plot in **Fig.7** and the polynomial Equation 14:

$$\text{Viscosity} = 29.19 + 6.34*X_1 - 7.24*X_2 - 7.35*X_3 - 4.55*X_4 - 0.549*X_1*X_2 - 0.993*X_1*X_3 - 0.326*X_1*X_4 - 5.72*X_2*X_3 - 4.06*X_2*X_4 - 3.60*X_3*X_4 + 0.539*(X_1)^2 - 4.58*(X_2)^2 - 2.42*(X_3)^2 - 2.27*(X_4)^2 \quad \textbf{(Eq.14)}$$

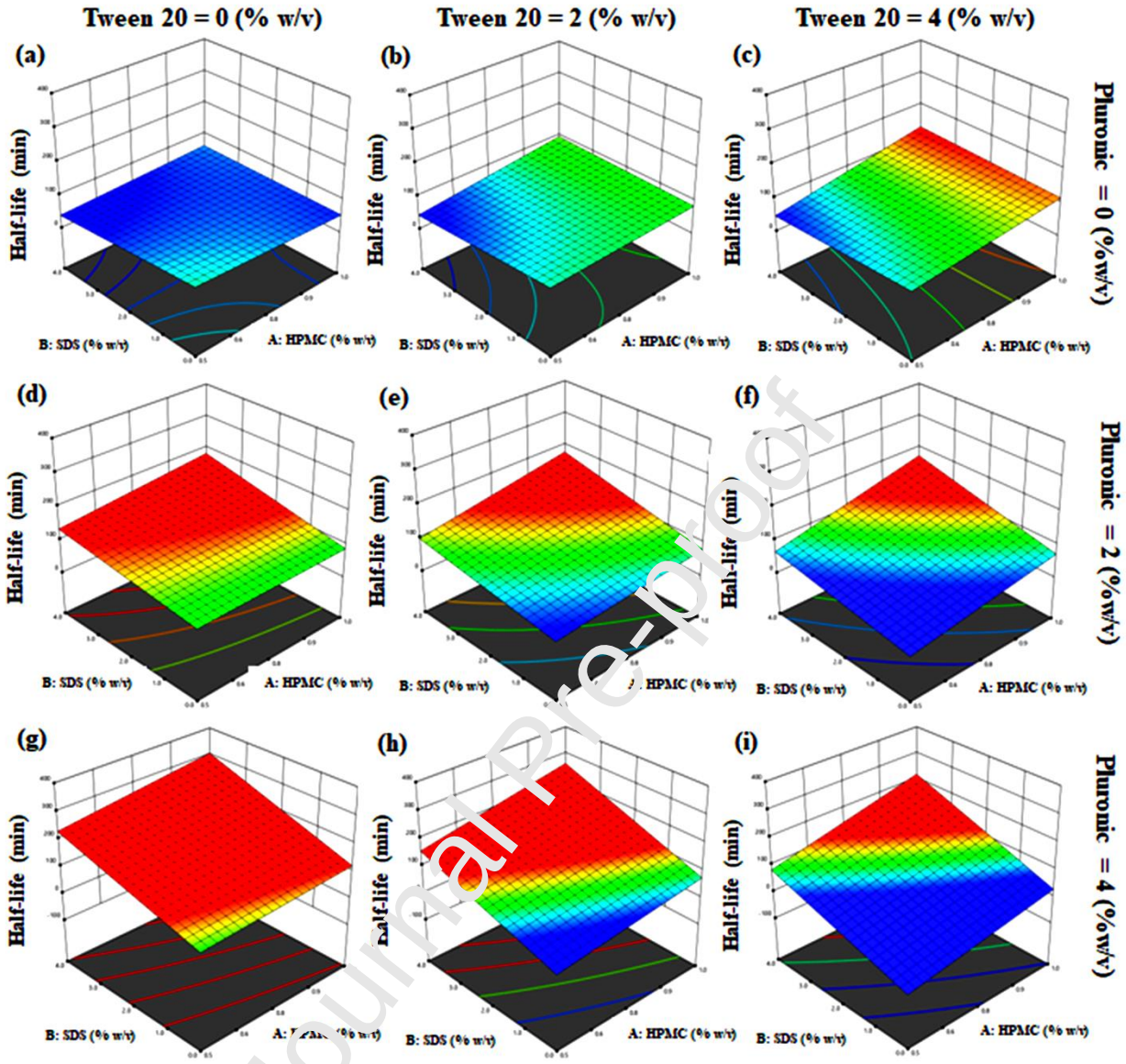

Fig.6. 3D plots of half-life response corresponding to different variable levels; **pluronic low level:** 0% (w/v) with different concentration (% w/v) of Tween 20 (a) 0, (b) 2, (c) 4, **pluronic medium level:** 2% (w/v) with different concentration (% w/v) of Tween 20 (d) 0, (e) 2, (f) 4, **pluronic high level:** 4% (w/v) with different concentration (% w/v) of Tween 20 (g) 0, (h) 2, (i) 4.

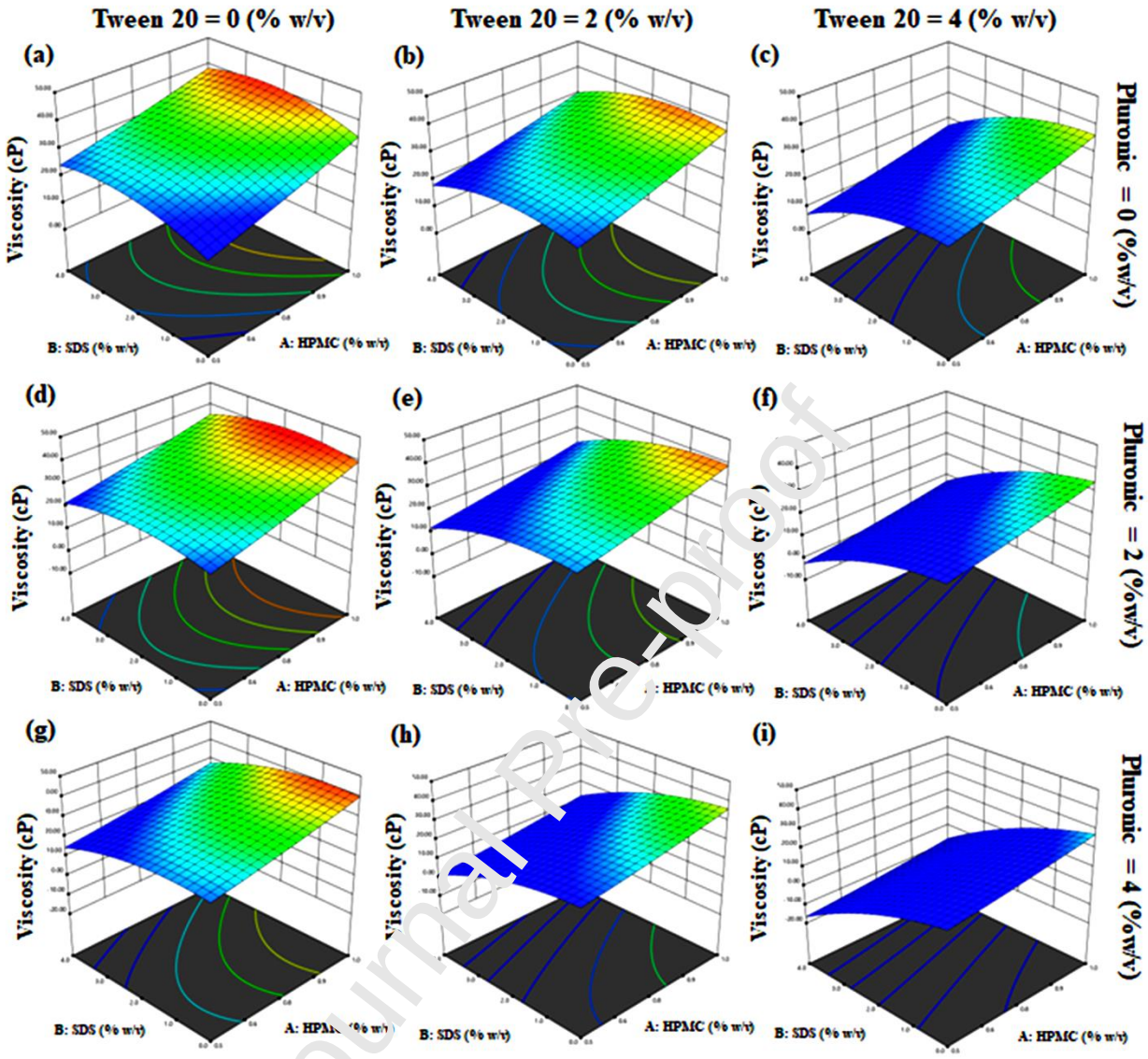

Fig.7. 3D plots of viscosity response corresponding to different variable levels; **pluronic low level:** 0% (w/v) with different concentration (% w/v) of Tween 20 (a) 0, (b) 2, (c) 4, **pluronic medium level:** 2% (w/v) with different concentration (% w/v) of Tween 20 (d) 0, (e) 2, (f) 4, **pluronic high level:** 4% (w/v) with different concentration (% w/v) of Tween 20 (g) 0, (h) 2, (i) 4.

3.3.2. Optimization of foam using D-optimal design

The desirability function established a suitable property in experimental design to achieve an optimum selection of evaluated variables. Optimization of foam concerning maximizing FE%, FVS%, foam half-life, and viscosity along with minimizing FLS%. As depicted in **Fig.8a-b**, contour plots of desirability and graphical optimization visualize the formulation design space. The suggested foam optimum formula consists of 1%(w/v) HPMC, 1.249%(w/v) SDS, 4%(w/v)

pluronic with the higher desirability of 0.935. The observed responses of the experimental trial were 183.3%, 82.35%, 16.6%, 170 min, and 42.2 cP, while predicted values were 180.57%, 89.47%, 17.24 %, 178.4 min, and 40.09 cP, for FE, FVS, FLS, half-life, and viscosity respectively.

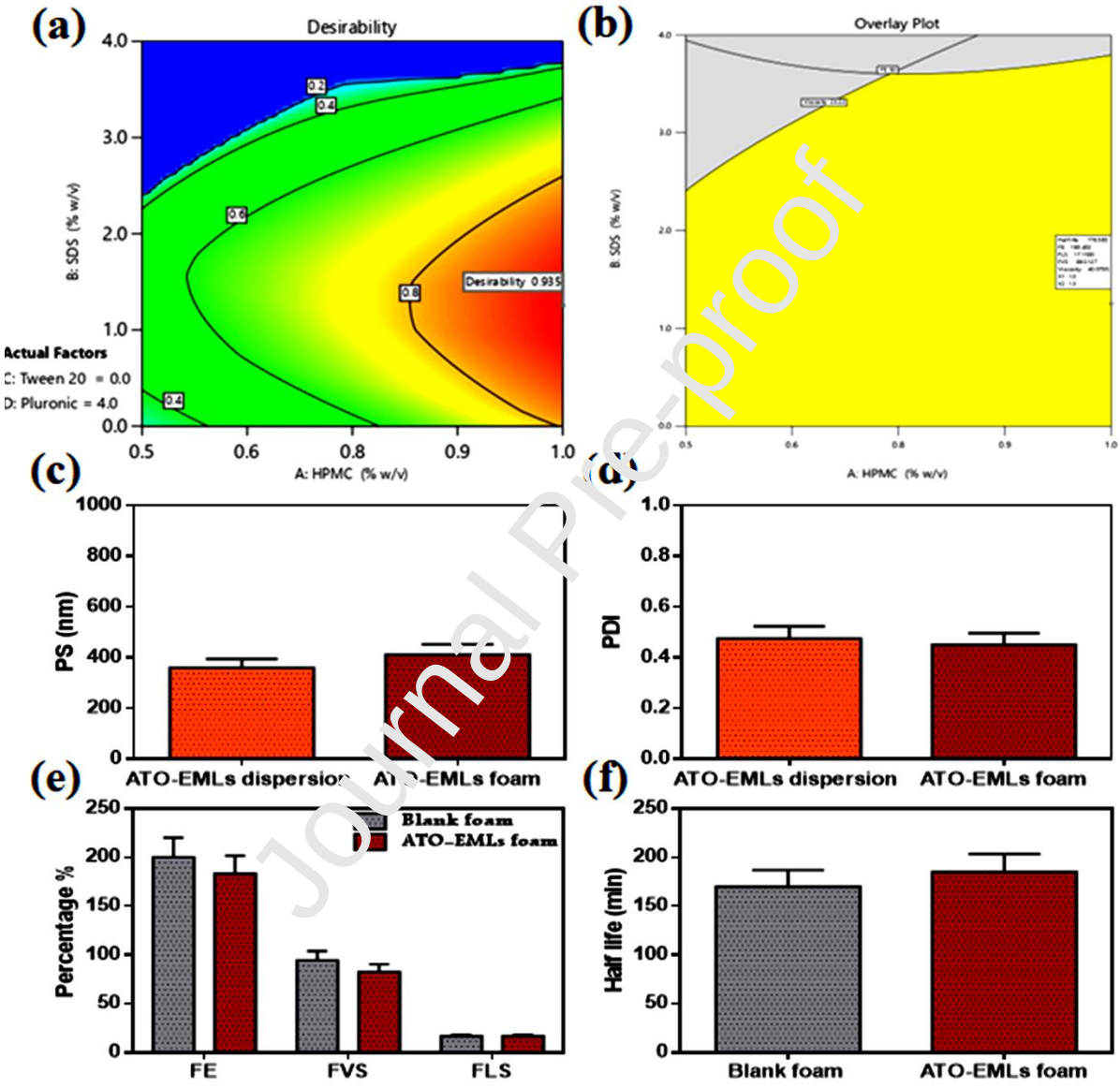

Fig.8. Design optimization model concerning variables and targeted responses; (a) desirability contour plot, (b) graphical optimization contour plot, **Comparative study** of ATO-EMLs foam with vesicle dispersion and blank foam regarding (c) Particle size, (d) Polydispersity index, (e) Foam calculated parameters, (f) and foam half-life; revealed insignificant differences as loaded foam conserve the optimum specifications.

3.4. Characterization of optimum ATO-EMLs foam formulation

3.4.1. Comparative study with ATO-EMLs and blank foam

To confirm the system's suitability after incorporating ATO-EML in foam optimum preparation, specific features for vesicle and foam were assessed to detect any variability. Khan et al. reported that different physicochemical properties of nanoparticles as particle size influence topical drug delivery, therefore PS and PDI were investigated to track any significant differences (Khan et al., 2022). Illustration in **Fig.8c-d** after data analysis showed slight changes with insignificant effects. Moreover, loaded foam stability was determined by calculated parameters as previously discussed in **section.3.3.1.**, which reflect stable foam formulation with insignificant changes in comparison with blank foam preparation **(Fig.8e-f)**.

3.4.2. Foam collapse

Foam collapse capability can estimate foam stability, as a long collapse time indicate good thermal stability (Parsa et al., 2019). As shown in **Fig.9a**, the performance of foam collapse during different time intervals estimates good stability with higher collapse time. Concerning breakability, the aqueous prepared foam belonged to the category of breakable foams which acquired stable attributes breaking by shear force (Farias et al., 2021). As reported by Tamarkin, breakable foam allows convenient dermal application with optimum administration as it retains stability for a suitable period. Preferably, the foam structure should be maintained stable for more than 2-3 minutes (Tamarkin, 2016).

3.4.3. Bubble size estimation

As illustrated in **Fig.9b**, after analyzing the image of foam bubbles by ImageJ software, the resulting histogram showed small relatively monodispersed bubbles. Bubble size and distribution affect foam application as a result of influence on rheological and stability patterns. Noticing by Mirtič et al., that the distribution impact is more pronounced as the unequal pattern may cause foam destabilization. Furthermore, the higher SDS concentration may result in small bubbles with homogenous distribution (Mirtič et al., 2017).

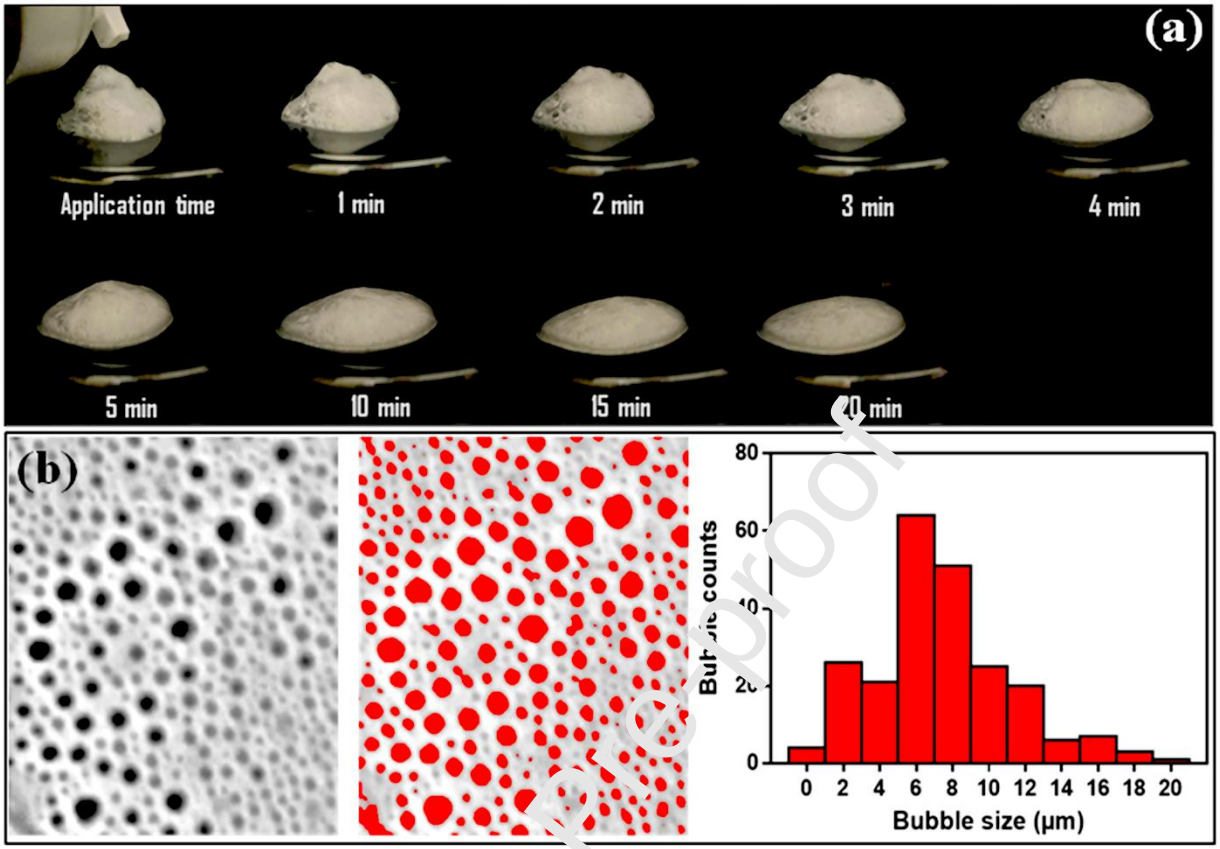

Fig.9. (a) Depicted foam collapse time from the side view after actuating; showing good stable structure with a long collapse time, (b) measured and analyzed bubble size and distribution using ImageJ software.

3.4.4. *In-vitro* release study

The release profile of ATO dispersion, ATO-EML best formula, and optimized ATO-EMLs foam system are graphically illustrated in **Fig.10a**, ATO showed a fast release pattern from the dispersion as 66% released within the first 12 hours, followed by completion achieved after 24 h. Otherwise, ATO-EML vesicles revealed a slow manner as almost only 25% of the drug was released after 24 hours, then reached 68% within 72 hours. The performance of ATO-EML formula reflects controlled and sustained release, which may be interpreted by emulsome core-shell structure as lipophilic drugs should confront a diffusion from the lipid core followed by the barrier of phospholipid membrane before drug release as per reported by Zhou and Chen. (Zhou and Chen, 2015). In another hand, only 50% of the drug in the foam system was released after 72 hours in a controlled manner, this may be explained according to foam composition as reported by Zhao et al., surfactants like pluronic increase drug solubility and cause a reduction in the release rate (Zhao et al., 2010a). Drug dispersion and ATO-EML formula release performance relevant to zero order kinetics which was estimated as the best fitting model due to higher R^2 that were 0.9910 and 0.9960, respectively. Zero order describes the system when the drug showed slow release (Elbaz et al., 2016), and the release rate is concentration-independent. Otherwise,

the ATO-EML foam system was relatively fitted to the Hixson Crowell model with an R^2 of 0.9726.

3.4.5. Stability study

No remarkable sedimentation or aggregation appeared by visual inspection of the ATO-EML foam solution for 6 months with the proper performance of foam production by using the actuator. Furthermore, measured parameters revealed an insignificant alteration in comparison to the freshly prepared sample ($p > 0.05$) as illustrated in **Fig.10b-d**, Stability attributes may refer to foam system composition which contains different stabilizing agents such as glycerin(Rial et al., 2014).

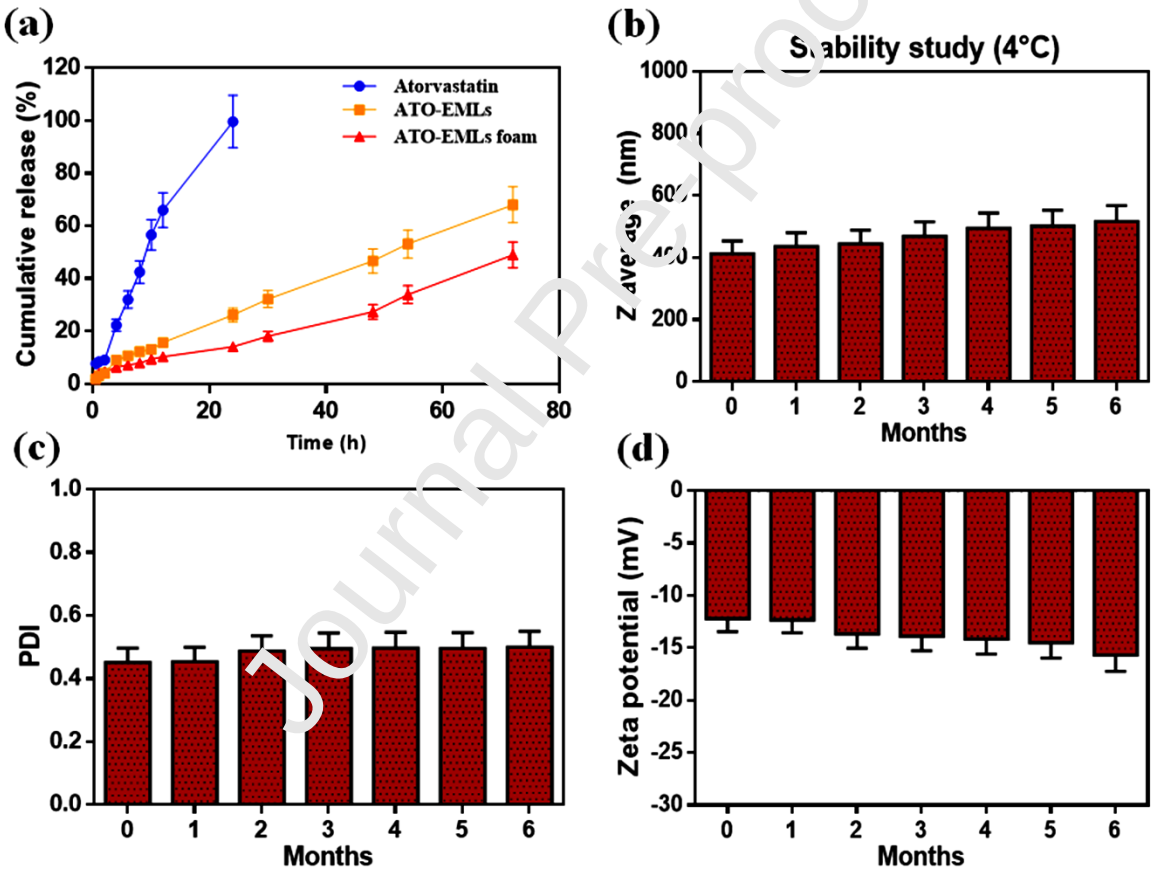

Fig. 10. (a) **Release study** illustrated as cumulative percentage of atorvastatin free drug in comparison to optimized ATO-EMLs before and after incorporation in foam system, **Stability study for 6 months**, evaluated sample storage at 4°C represented by (b) Particle size, (c), polydispersity index, and (d) Zeta potential; reflect stable attributes with no significant difference in comparison to fresh sample.

3.5. *In-vivo* permeation visualization using confocal laser scanning microscopy

Skin potential entry routes rely on hair follicles alongside with sebaceous gland, trans-appendageal, and sweat duct. Follicles and sebaceous gland lipidic nature established a favorable route for lipophilic drug penetration (Kováčik et al., 2020). Localization of Emulsome-foam system in skin layers detected by applied FDA- loaded formulation and tracking fluorescence intensity. CLSM study showed obvious higher intensity indicating good system permeation as depicted in **Fig.11**. Accumulation of fluorescence in skin tissue was evaluated quantitatively as shown in **Fig.11.d** to simulate permeation of the ATO-EMLs foam system concerning deep layers. Employed nanovesicles in topical therapy of fungus infection, enhance deep penetration resulting in promising clinical results (Deaguero et al., 2020).

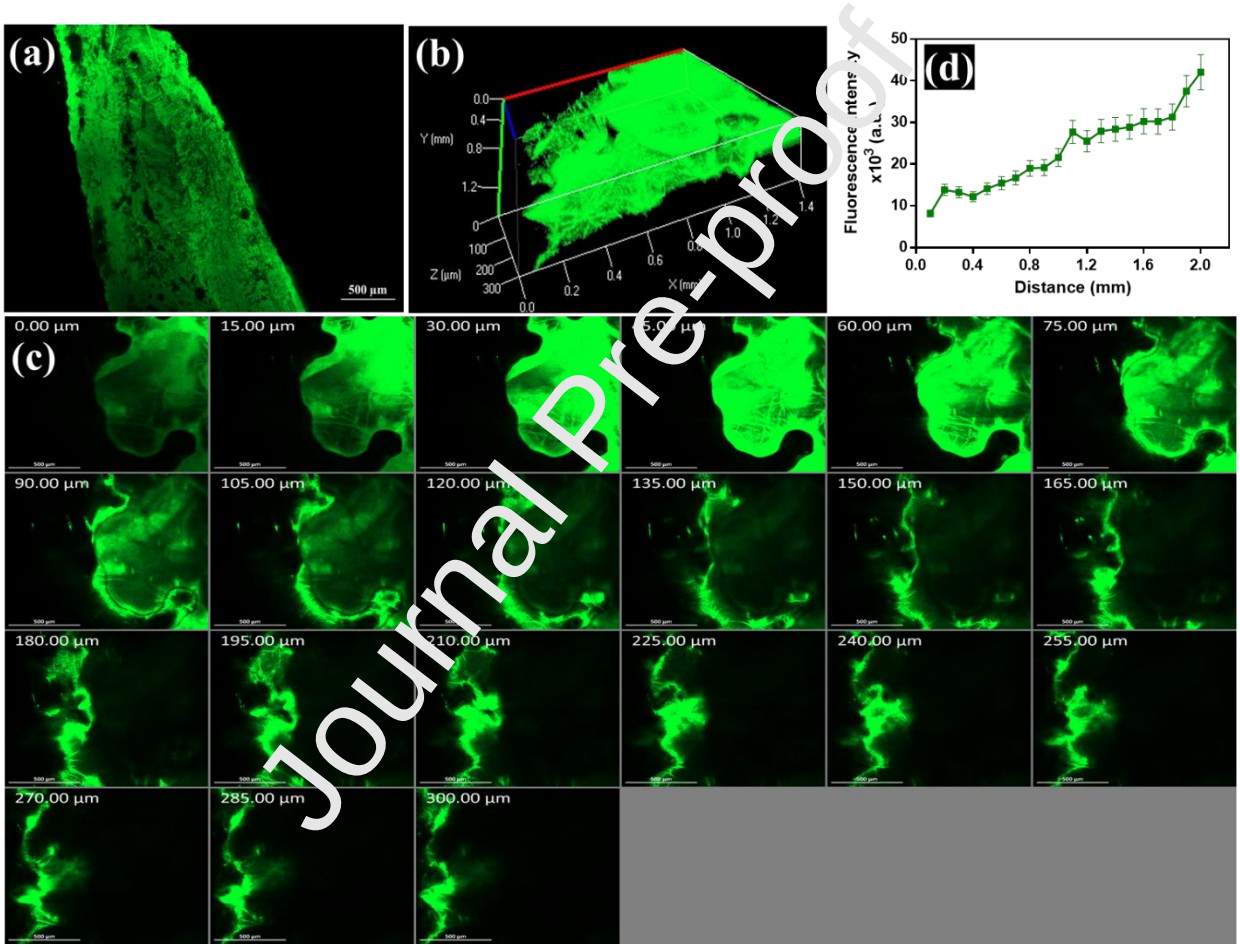

Fig. 11. Confocal laser scanning microscopy images of EMLs-foam system (a) tile x-y image of skin treated with FDA-loaded emulsome foam system, (b) 3D plot using z-stack images of the skin section from 0 µm to 300 µm, and (c) sequential images from 0-300 µm with 15 µm increments showed that penetration occurred across different skin layers revealed with high fluorescence intensity, (d) quantitative measurement of fluorescence intensity profile across skin layers.

3.6. *In-vitro* microbiology study

3.6.1. Micro-Well dilution method

As represented in **Fig.12a-b**, optical densities were measured for two fungal species. MIC values for *C. albicans* were 650 µg/ml when evaluating the free ATO, otherwise, drug incorporation in the emulsome foam system reduced the MIC to 350 µg/ml (**Fig.12c**). The foam system was similar to the calculated result of the commercial drug, in addition, the blank-EMLs foam MIC was 750 µg/ml. The *A. fumigatus* remarked higher MIC values of 850 µg/ml for the free ATO, in addition to 650 µg/ml, and 550 µg/ml for the blank and loaded ATO-emulsome foam system respectively. The MIC of the commercial drug regarding A. *fumigatus* was 550 µg/ml.

3.6.2. Well diffusion method

The diameter of inhibition zones was illustrated in **Fig.12d** for *C. albicans* and *A. fumigatus*. Regarding *C. albicans*, the ATO- EML foam system was more sensitive obviously than the free ATO as the zone measured were 37 and 26 mm respectively **(Fig.12e,f)**. While blank-EML foam showed only 22 mm in diameter **(Fig. 12g)** The loaded foam system showed a close value to the commercial drug with preference as the latter zone diameter was 35mm **(Fig. 12h)**. In contrast, the *A. fumigatus* measured diameters reflected lower sensitivity than *C. albicans* to the drug and prepared formulae. The inhibition zone was 22 mm of the free ATO and 28 mm after its incorporation into the EML-foam system **(Fig. 12i,j)**, while the blank system was 24 mm in diameter **(Fig. 12k)**. The highest zone of inhibition was revealed for the commercial control of 30 mm **(Fig. 12l)**. A previous *in-vitro* study conducted by Mahmoud et al. on isolated candida strains, suggests atorvastatin as a promising antifungal drug, especially in combinations. The antifungal activity upholds by microdilution and diffusion methods (Mahmoud et al., 2021b). Furthermore, Ajdidi et al. reported a reduction in aspergillus growth by atorvastatin-inhibiting effect and remarked elevation in membrane permeability proved by the detection of the augmented release of cell proteins (Ajdidi et al., 2020). The observed antifungal activity in the blank-EML foam system was explained by SDS-fungal growth inhibition noticed by Woertz and Kinney (Woertz and Kinney, 2004).

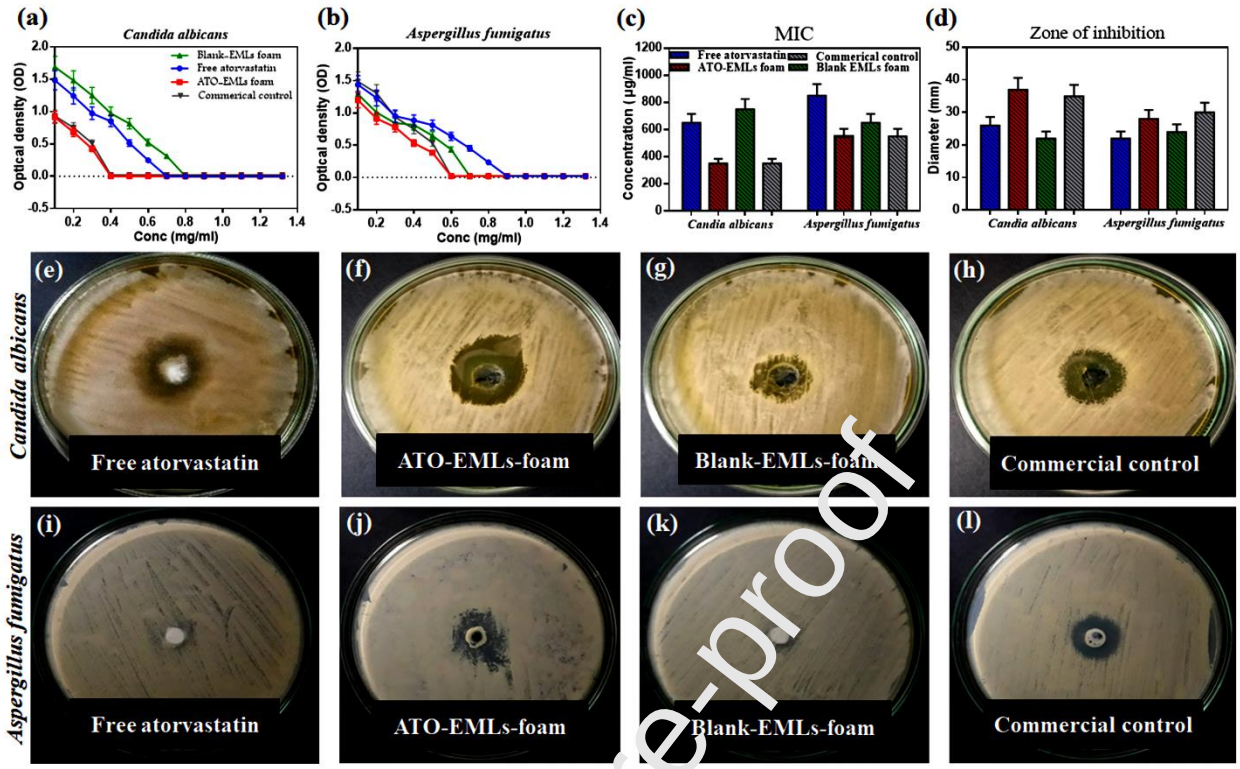

Fig.12. *In-vitro* microbiology studies: In way to determine MIC; optical density values of two fungal species against the diluted concentration of the evaluated samples were determined (a) *C.albicans*, (b) *A.fumigatus*, the susceptibility of isolated fungal species to atorvastatin, blank and ATO-loaded EMLs foam in addition to commercial control was estimated through measured (c) MIC values, (d) diameters of inhibition zone, inhibition zones on C. albicans were visualized for (e) Atorvastatin, (f) ATO-EMLs foam, (g) blank-EML foam, (h) Commercial control, inhibition zones on *A.fumigatus* were visualized for (i) Atorvastatin, (j) ATO-EMLs foam, (k) Blank-EML foam, (l) Commercial control.

3.7. *In-vivo* Study

3.7.1. Biocompatibility Study

Histopathological examination of skin samples from different groups was conducted to evaluate the biocompatibility of the developed formula. a normal skin specimen was obtained from a normal rat as shown in **Fig.13a.** Normal skin shows the two layers of the skin, the epidermis (**Fig.13a** E) and the dermis (**Fig.13a** D). The dermis shows an outer papillary layer (**Fig.13a** P), an inner reticular layer (**Fig.13a** R). **Fig.13b** demonstrated the placebo foam after 1 week. Focal areas of epidermal discontinuation (**Fig.13b** arrow) due to loss of superficial epidermal cell layers (erosion) and hair follicles (**Fig.13b** H) The dermis shows focal areas of collagen loss or empty space (**Fig.13b** **) of variable sizes. Perifollicular and intrafollicular infiltration of neutrophils, lymphocytes, and mononuclear cellular infiltration in the dermis (**Fig.13b** *). Many hair follicles (**Fig.13b** H) with an absence of associated sebaceous glands are observed.

Hyperkeratosis (**Fig.13b** K). **Fig.13c** demonstrated the placebo foam after 3 weeks. The dermis shows focal areas of collagen loss or empty space (**Fig.13c** **) of variable sizes. The stratum corneum consists of many layers of flattened non-cellular acidophilic keratin scales (**Fig.13c** SC). The epidermis (**Fig.13c** E) is seen in this figure. The dermis can be broken down into two distinct layers, the outside papillary layer (**Fig.13c** P) and an inner reticular layer (**Fig.13c** R). **Fig.13d** demonstrated the ATO-EML foam after 1 week. The epidermis (**Fig.13d** E) is seen in this figure. Hair follicles related to sebaceous glands (**Fig.13d** arrow) can be seen in the dermis' outer papillary layer (**Fig.13d** P) and an inner reticular layer (**Fig.13d** R). Flattened non-cellular acidophilic keratin scales cover most of the stratum corneum (**Fig.13d** bold arrow). **Fig.13e** demonstrated the ATO-EML foam after 3 weeks. The epidermis (**Fig.13e** E) may be seen here. The dermis can be broken down into two distinct layers, the outside papillary layer (**Fig.13e** P), and the inner reticular layer (**Fig.13e** R). There was a hair follicle (**Fig.13e** arrowhead). The stratum corneum is made up of multiple layers of keratin scales that are non-cellular and acidophilic and have been flattened (**Fig.13e** bold arrow). Mononuclear cellular infiltration in the dermis (*) was detected. In conclusion, after three weeks period from the application of both placebo foam and ATO-EML foam, the placebo foam showed an increase in hyperkeratosis and inflammation after 1 week but after 3 weeks slight progress in epidermal hypertrophy was noticed. On the other hand, ATO-EML foam after 3 weeks demonstrated improvement in hyperkeratosis, inflammation, epidermal hypertrophy, fibrosis, and follicle hyperplasia. These observations suggest that the unloaded and loaded foam have an initial undesirable effect on skin layers due to the presence of different surfactants followed by slightly returning to normal after treatment ends.

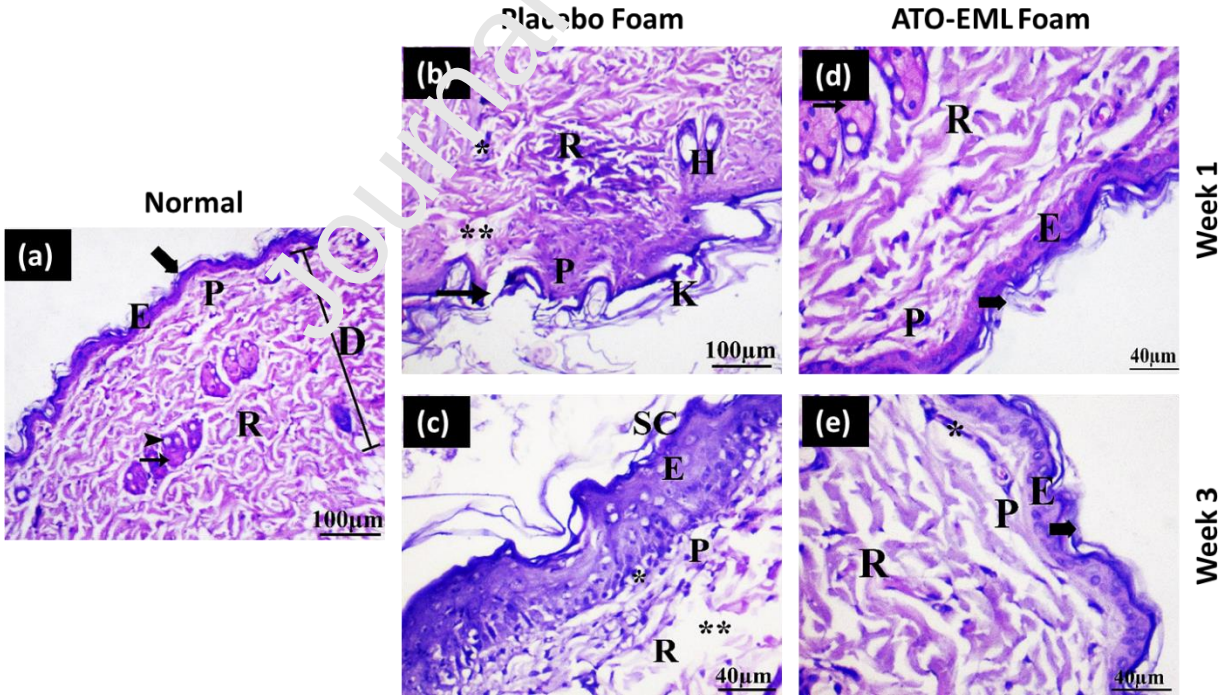

Fig.13. *In-vivo* biocompatibility study: (a) Normal skin, **(b)** placebo foam after 1 week, **(c)** placebo foam after 3 weeks, **(d)** ATO-EML foam after 1 week, **(e)** ATO-EMLs after 3 weeks.

3.7.2. Microbiology Study

The *in-vivo* dermal fungal infection rat model was conducted using *Candida Albicans* to compare the activity of a standard drug (Terbinafine HCl) with ATO-EML foam. After 3 weeks, the positive control group demonstrated redness under the skin (**Fig. 14a**). The Terbinafine HCl group showed normal skin (**Fig. 14b**). The ATO-EML foam showed slight redness under the skin (**Fig. 14c**). A microbial count for infected skin was measured. The positive control group showed a colony count of 9.23E+06 CFU/mL, which was significantly higher than the Terbinafine HCl group with a colony count of 4.07E+04 CFU/mL (**** $p < 0.0001$) and higher than ATO-EML foam group with a colony count of 4.67E+05 CFU/mL (**** $p < 0.0001$) as shown in **Fig. 14d**. The histopathological examination of skin samples was conducted as shown in **Fig. 14e-g**. The positive control group showed hyperkeratosis (**Fig. 14e** K) Perifollicular and intrafollicular infiltration of neutrophils, lymphocytes, and mononuclear cellular infiltration in the dermis (**Fig. 14e** *). The standard group showed hyperkeratosis (**Fig. 14f** K) Perifollicular and intrafollicular infiltration of neutrophils, lymphocytes, and mononuclear cellular infiltration in the dermis (**Fig. 14f** *). The dermis shows an outer papillary layer (**Fig. 14f** P), an inner reticular layer (**Fig. 14f** R), hair follicles (**Fig. 14f** H) and Sebaceous glands (**Fig. 14f** SG). the ATO-EML foam group hyperkeratosis (**Fig. 14g** K), normal epidermis thickness (**Fig. 14g** E), perifollicular and intrafollicular infiltration of neutrophils, lymphocytes, mononuclear cellular infiltration in the dermis (**Fig. 14g** *), and increased cellular proliferation (hyperplasia) of some hair follicles as a follicular bulge (**Fig. 14g** curved arrow). The ATO-EML foam group demonstrated a mild thick keratin layer, mild inflammatory cells with many hair follicles and sebaceous glands in the dermis, normal thickness epidermal areas, and a mild rate of cyst follicles. These findings indicated that the skin gradually returns to normal with the eradication of infection as a result of treatment with ATO-EML foam.

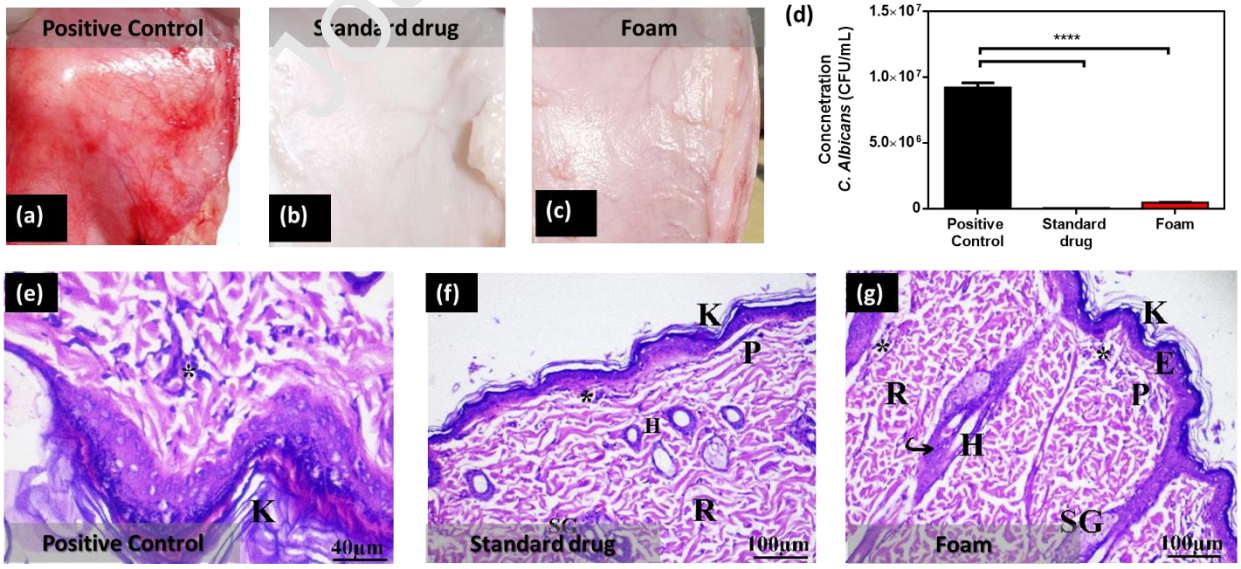

Fig.14. ***In-vivo*** **microbiological study:** photographic images of the infected skin area of rat dorsal **(a)** positive control group, **(b)** standard drug group, and **(c)** ATO-EML foam group. **(d)** *C. Albicans* concentration in CFU/mL of different groups (**** $p < 0.0001$). Histopathological evaluation: **(e)** Positive group, **(f)** Standard drug group, **(g)** ATO-EML foam.

4. Conclusion

Atorvastatin (ATO) revealed positive results that confirm its activity as an antifungal candidate while using optimized ATO-emulsome vesicle incorporated in foam formulation. The emulsome showed a suitable and applicable carrier for ATO dermal application with higher desirable responses while using 22.5mg cholesterol and probe sonication for 15min . The optimized foam system (containing 1%HPMC, and 1.249%SDS with 4%pluronic as SAA) reduced the drug release rate in a controlled manner as only 50% of ATO was released after 72 hours. Although foam system uphold storage stability in the refrigerator for a long period with insignificant alteration in comparison to the freshly prepared sample. Moreover, the assessment of foam collapse time and bubble size reflected foam system stability at the site of application, as small bubbles size and homogenous distribution reinforece stability with higher collapse time. Furthermore, a visualization study using CLSM remarked higher drug permeation via skin tissues. The conducted *in-vitro* and *in-vivo* microbiology studies reinforced the drug's antifungal activity and showed promising outcomes of ATO emulsome foam formula.

5. Conflict of Interest

The authors declare that they have no known competing financial interests or personal relationships that could have appeared to influence the work reported in this paper.

6. Funding Sources

This work was supported by the Science, Technology & Innovation Funding Authority (STIFA/STDF) under grant number 30084 (PI Islam A. Khalil).

7. Author Contributions

Alaa S. Eita: methodology, data curation, formal analysis, investigation, writing-original draft, writing-review and editing, and visualization. **Amna M. A. Makky**: conceptualization, methodology, writing-original draft, writing-review and editing. **Asem Anter**: methodology, data curation, formal analysis, investigation. **Islam A. Khalil**: conceptualization, methodology, data curation, formal analysis, investigation, writing-original draft, writing-review and editing, visualization, funding acquisition, and project administration.

8. References

Abdellatif, M.M., Khalil, I.A., Elakkad, Y.E., Eliwa, H.A., Samir, T., Al-Mokaddem, A.K., 2020. Formulation and Characterization of Sertaconazole Nitrate Mucoadhesive Liposomes for Vaginal Candidiasis. Int. J. Nanomedicine Volume 15, 4079–4090. https://doi.org/10.2147/IJN.S250960

Abdellatif, M.M., Khalil, I.A.F., Khalil, M.A.F., 2017. Sertaconazole nitrate loaded nanovesicular systems for targeting skin fungal infection: In-vitro, ex-vivo and in-vivo evaluation. Int. J. Pharm. 527, 1–11. https://doi.org/10.1016/j.ijpharm.2017.05.029

Aburahma, M.H., Badr-Eldin, S.M., 2014. Compritol 888 ATO: a multifunctional lipid excipient in drug delivery systems and nanopharmaceuticals. Expert Opin. Drug Deliv. 11, 1865–1883. https://doi.org/10.1517/17425247.2014.935335

Ajdidi, A., Sheehan, G., Kavanagh, K., 2020. Exposure of Aspergillus fumigatus to Atorvastatin Leads to Altered Membrane Permeability and Induction of an Oxidative Stress Response. J. Fungi 6, 42. https://doi.org/10.3390/jof6020042

Albash, R., Elmahboub, Y., Baraka, K., Abdellatif, M.M., Alaa-Eldin, A.A., 2020. Ultra-deformable liposomes containing terpenes (terpesomes) loaded fenticonazole nitrate for treatment of vaginal candidiasis: Box-Behnken design optimization, comparative ex vivo and in vivo studies. Drug Deliv. 27, 1514–1528. https://doi.org/10.1080/10717544.2020.1837295

Aldawsari, Hibah M, Ahmed, O.A.A., Alhakamy, N.A., Neamatallah, T., Fahmy, U.A., Badr-Eldin, S.M., 2021. Lipidic Nano-Sized Emulsomes Potentiates the Cytotoxic and Apoptotic Effects of Raloxifene Hydrochloride in MCF-7 Human Breast Cancer Cells: Factorial Analysis and In Vitro Anti-Tumor Activity Assessment. Pharmaceutics 13, 783. https://doi.org/10.3390/pharmaceutics13060783

Aldawsari, Hibah M., Ahmed, O.A.A., Alhakamy, N.A., Neamatallah, T., Fahmy, U.A., Badr-Eldin, S.M., 2021. Lipidic Nano-Sized Emulsomes Potentiates the Cytotoxic and Apoptotic Effects of Raloxifene Hydrochloride in MCF-7 Human Breast Cancer Cells: Factorial Analysis and In Vitro Anti-Tumor Activity Assessment. Pharmaceutics 13, 783. https://doi.org/10.3390/pharmaceutics13060783

Alyousef, A.A., 2021. Antifungal Activity and Mechanism of Action of Different Parts of Myrtus communis Growing in Saudi Arabia against Candida Spp. J. Nanomater. 2021, 1–10. https://doi.org/10.1155/2021/3484125

Arzhavitina, A., Steckel, H., 2010a. Foams for pharmaceutical and cosmetic application. Int. J. Pharm. 394, 1–17. https://doi.org/10.1016/j.ijpharm.2010.04.028

Arzhavitina, A., Steckel, H., 2010b. Foams for pharmaceutical and cosmetic application. Int. J. Pharm. 394, 1–17. https://doi.org/10.1016/j.ijpharm.2010.04.028

Awan, Z.A., A. Fahmy, U., Badr-Eldin, S.M., Ibrahim, T.S., Asfour, H.Z., Al-Rabia, M.W., Alfarsi, A., Alhakamy, N.A., Abdulaal, W.H., Al Sadoun, H., Helmi, N., Noor, A.O., Caraci, F., Almasri, D.M., Caruso, G., 2020. The Enhanced Cytotoxic and Pro-Apoptotic Effects of Optimized Simvastatin-Loaded Emulsomes on MCF-7 Breast Cancer Cells.

Pharmaceutics 12, 597. https://doi.org/10.3390/pharmaceutics12070597

Bai, T., Liu, Y., Liu, J., Yu, C., Jiang, W., Fan, Y., 2019. A comparison of different surfactants on foam stability in foam sclerotherapy in vitro. J. Vasc. Surg. 69, 581-591.e1. https://doi.org/10.1016/j.jvs.2018.02.033

Beg, S., Swain, S., Rahman, M., Hasnain, M.S., Imam, S.S., 2019. Application of Design of Experiments (DoE) in Pharmaceutical Product and Process Optimization, in: Pharmaceutical Quality by Design. Elsevier, pp. 43–64. https://doi.org/10.1016/B978-0-12-815799-2.00003-4

Bera, A., Ojha, K., Mandal, A., 2013. Synergistic Effect of Mixed Surfactant Systems on Foam Behavior and Surface Tension. J. Surfactants Deterg. 16, 621–630. https://doi.org/10.1007/s11743-012-1422-4

Bolat, Z.B., Islek, Z., Demir, B.N., Yilmaz, E.N., Sahin, F., Ucisik, M.H., 2020. Curcumin- and Piperine-Loaded Emulsomes as Combinational Treatment Approach Enhance the Anticancer Activity of Curcumin on HCT116 Colorectal Cancer Model. Front. Bioeng. Biotechnol. 8, 1–21. https://doi.org/10.3389/fbioe.2020.00050

Bradbury, P., Traini, D., Ammit, A.J., Young, P.M., Ong, H.X., 2018. Repurposing of statins via inhalation to treat lung inflammatory conditions. Adv. Drug Deliv. Rev. 133, 93–106. https://doi.org/10.1016/j.addr.2018.06.005

Bureiko, A., Trybala, A., Kovalchuk, N., Starov, V., 2015. Current applications of foams formed from mixed surfactant–polymer solutions. Adv. Colloid Interface Sci. 222, 670–677. https://doi.org/10.1016/j.cis.2014.10.001

Cabral, M.E., Figueroa, L.I.C., Fariña, J.I., 2013. Synergistic antifungal activity of statin–azole associations as witnessed by Saccharomyces cerevisiae- and Candida utilis-bioassays and ergosterol quantification. Rev. Iberoam. Micol. 30, 31–38. https://doi.org/10.1016/j.riam.2012.09.006

Camilo, C.J.J., Leite, D.O.D., Silva, A.R.A., Menezes, I.R.A., Coutinho, H.D.M., Costa, J.G.M., 2020. Lipid vesicles: applications, principal components and methods used in their formulations: A review. Acta Biológica Colomb. 25, 339–352. https://doi.org/10.15446/abc.v25n2.74830

Carey, E., Stubenrauch, C., 2010. Foaming properties of mixtures of a non-ionic (C12DMPO) and an ionic surfactant (C12TAB). J. Colloid Interface Sci. 346, 414–423. https://doi.org/10.1016/j.jcis.2010.03.013

Costa, P., Sousa Lobo, J.M., 2001. Modeling and comparison of dissolution profiles. Eur. J. Pharm. Sci. 13, 123–133. https://doi.org/10.1016/S0928-0987(01)00095-1

da Silva, E.P., Pereira, M.A.V., de Barros Lima, I.P., Lima, N.G.P.B., Barbosa, E.G., Aragão, C.F.S., Gomes, A.P.B., 2016. Compatibility study between atorvastatin and excipients using DSC and FTIR. J. Therm. Anal. Calorim. 123, 933–939. https://doi.org/10.1007/s10973-015-5077-z

Danaei, M., Dehghankhold, M., Ataei, S., Hasanzadeh Davarani, F., Javanmard, R., Dokhani, A., Khorasani, S., Mozafari, M., 2018. Impact of Particle Size and Polydispersity Index on the

Clinical Applications of Lipidic Nanocarrier Systems. Pharmaceutics 10, 57. https://doi.org/10.3390/pharmaceutics10020057

de Oliveira Neto, A.S., Souza, I.L.A., Amorim, M.E.S., de Freitas Souza, T., Rocha, V.N., do Couto, R.O., Fabri, R.L., de Freitas Araújo, M.G., 2021. Antifungal efficacy of atorvastatin-containing emulgel in the treatment of oral and vulvovaginal candidiasis. Med. Mycol. 59, 476–485. https://doi.org/10.1093/mmy/myaa071

Deaguero, I.G., Huda, M.N., Rodriguez, V., Zicari, J., Al-Hilal, T.A., Badruddoza, A.Z.M., Nurunnabi, M., 2020. Nano-Vesicle Based Anti-Fungal Formulation Shows Higher Stability, Skin Diffusion, Biosafety and Anti-Fungal Efficacy In Vitro. Pharmaceutics 12, 516. https://doi.org/10.3390/pharmaceutics12060516

Derikvand, Z., Riazi, M., 2016. Experimental investigation of a novel foam formulation to improve foam quality. J. Mol. Liq. 224, 1311–1318. https://doi.org/10.1016/j.molliq.2016.10.119

Eftekhari, A.A., Farajzadeh, R., 2017. Effect of Foam on Liquid Phase Mobility in Porous Media. Sci. Rep. 7, 43870. https://doi.org/10.1038/srep43870

El-Zaafarany, G., Soliman, M., Mansour, S., Cespi, M., Palmieri, G., Illum, L., Casettari, L., Awad, G., 2018. A Tailored Thermosensitive PLGA-PEG-PLGA/Emulsomes Composite for Enhanced Oxcarbazepine Brain Delivery via the Nasal Route. Pharmaceutics 10, 217. https://doi.org/10.3390/pharmaceutics10040217

El-Zaafarany, G.M., Soliman, M.E., Mansour, S., Awad, G.A.S., 2016. Identifying lipidic emulsomes for improved oxcarbazepine brain targeting: In vitro and rat in vivo studies. Int. J. Pharm. 503, 127–140. https://doi.org/10.1016/j.ijpharm.2016.02.038

Elbaz, N.M., Khalil, I.A., Abd-Rabou, A.A., El-Sherbiny, I.M., 2016. Chitosan-based nano-in-microparticle carriers for enhanced oral delivery and anticancer activity of propolis. Int. J. Biol. Macromol. 92, 254–269. https://doi.org/10.1016/j.ijbiomac.2016.07.024

Fahmy, U.A., Aldawsari, H.M., Badr-Eldin, S.M., Ahmed, O.A.A., Alhakamy, N.A., Alsulimani, H.H., Caraci, F., Caruso, G., 2020. The Encapsulation of Febuxostat into Emulsomes Strongly Enhances the Cytotoxic Potential of the Drug on HCT 116 Colon Cancer Cells. Pharmaceutics 12, 956. https://doi.org/10.3390/pharmaceutics12100956

Farkas, D., Kállai-Szabó, N., Antal, I., 2019. Foams as carrier systems for pharmaceuticals and cosmetics. Acta Pharm. Hung. 89, 5–15. https://doi.org/10.33892/aph.2019.89.5-15

Farkas, D., Kállai-Szabó, N., Sárádi-Kesztyűs, Á., Lengyel, M., Magramane, S., Kiss, É., Antal, I., 2021. Investigation of propellant-free aqueous foams as pharmaceutical carrier systems. Pharm. Dev. Technol. 26, 253–261. https://doi.org/10.1080/10837450.2020.1863426

Gennari, C.G.M., Selmin, F., Minghetti, P., Cilurzo, F., 2019. Medicated Foams and Film Forming Dosage Forms as Tools to Improve the Thermodynamic Activity of Drugs to be Administered Through the Skin. Curr. Drug Deliv. 16, 461–471. https://doi.org/10.2174/1567201816666190118124439

Ghanem, H.A., Nasr, A.M., Hassan, T.H., Elkhoudary, M.M., Alshaman, R., Alattar, A., Gad, S., 2021. Comprehensive Study of Atorvastatin Nanostructured Lipid Carriers through

Multivariate Conceptualization and Optimization. Pharmaceutics 13, 178. https://doi.org/10.3390/pharmaceutics13020178

Gupta, A.K., Venkataraman, M., 2022. Antifungal resistance in superficial mycoses. J. Dermatolog. Treat. 33, 1888–1895. https://doi.org/10.1080/09546634.2021.1942421

Gupta, R., Gupta, M., Mangal, S., Agrawal, U., Vyas, S.P., 2014. Capsaicin-loaded vesicular systems designed for enhancing localized delivery for psoriasis therapy. Artif. Cells, Nanomedicine, Biotechnol. 44, 1–10. https://doi.org/10.3109/21691401.2014.984301

Gupta, U., Singh, V., Kumar, V., Khajuria, Y., 2014. Spectroscopic Studies of Cholesterol: Fourier Transform Infra-Red and Vibrational Frequency Analysis. Mater. Focus 3, 211–217. https://doi.org/10.1166/mat.2014.1161

Habib, B.A., Abdeltawab, N.F., Salah Ad-Din, I., 2022. D-optimal mixture design for optimization of topical dapsone niosomes: in vitro characterization and in vivo activity against Cutibacterium acnes. Drug Deliv. 29, 821–836. https://doi.org/10.1080/10717544.2022.2048131

Hassanabad, A.F., 2019. Current perspectives on statins as potential anti-cancer therapeutics: Clinical outcomes and underlying molecular mechanisms. Transl. Lung Cancer Res. 8, 692–699. https://doi.org/10.21037/tlcr.2019.09.08

Hughes, J., Rees, S., Kalindjian, S., Philpott, K., 2011. Principles of early drug discovery. Br. J. Pharmacol. 162, 1239–1249. https://doi.org/10.1111/j.1476-5381.2010.01127.x

Kamel, R., AbouSamra, M.M., Afifi, S.M., Galal, A.F., 2022. Phyto-emulsomes as a novel nano-carrier for morine hydrate to combat leukemia: In vitro and pharmacokinetic study. J. Drug Deliv. Sci. Technol. 103700. https://doi.org/10.1016/j.jddst.2022.103700

Kassem, A.A., Abd El-Alim, S.H., Asfour, M.H., 2017. Enhancement of 8-methoxypsoralen topical delivery via nanosized niosomal vesicles: Formulation development, in vitro and in vivo evaluation of skin deposition. Int. J. Pharm. 517, 256–268. https://doi.org/10.1016/j.ijpharm.2016.12.018

Khan, A.S., Shah, K.U., Mohtini, M. Al, Alsalman, A.J., Hawaj, M.A. Al, Alhashem, Y.N., Ghazanfar, S., Khan, K.A., Niazi, Z.R., Farid, A., 2022. Tacrolimus-Loaded Solid Lipid Nanoparticle Gel: Formulation Development and In Vitro Assessment for Topical Applications. Gels 8, 129. https://doi.org/10.3390/gels8020129

Khan, I., Needham, R., Yousaf, S., Houacine, C., Islam, Y., Bnyan, R., Sadozai, S.K., Elrayess, M.A., Elhissi, A., 2021. Impact of phospholipids, surfactants and cholesterol selection on the performance of transfersomes vesicles using medical nebulizers for pulmonary drug delivery. J. Drug Deliv. Sci. Technol. 66, 102822. https://doi.org/10.1016/j.jddst.2021.102822

Kováčik, A., Kopečná, M., Vávrová, K., 2020. Permeation enhancers in transdermal drug delivery: benefits and limitations. Expert Opin. Drug Deliv. 17, 145–155. https://doi.org/10.1080/17425247.2020.1713087

Kurowska, A., Ghate, V., Kodoth, A., Shah, Aarti, Shah, Abhishek, Vishalakshi, B., Prakash, B., Lewis, S.A., 2019. Non-Propellant Foams of Green Nano-Silver and Sulfadiazine:

Development and In Vivo Evaluation for Burn Wounds. Pharm. Res. 36, 122. https://doi.org/10.1007/s11095-019-2658-8

Mahdi, W.A., Bukhari, S.I., Imam, S.S., Alshehri, S., Zafar, A., Yasir, M., 2021. Formulation and Optimization of Butenafine-Loaded Topical Nano Lipid Carrier-Based Gel: Characterization, Irritation Study, and Anti-Fungal Activity. Pharmaceutics 13, 1087. https://doi.org/10.3390/pharmaceutics13071087

Mahmood, S., Taher, M., Mandal, U.K., 2014. Experimental design and optimization of raloxifene hydrochloride loaded nanotransfersomes for transdermal application. Int. J. Nanomedicine 9, 4331–46. https://doi.org/10.2147/IJN.S65408

Mahmoud, D.E., Faraag, A.H.I., Abu El-Wafa, W.M., 2021a. In vitro study on the potential fungicidal effects of atorvastatin in combination with some azole drugs against multidrug resistant Candida albicans. World J. Microbiol. Biotechnol. 37, 191. https://doi.org/10.1007/s11274-021-03158-4

Mahmoud, D.E., Faraag, A.H.I., Abu El-Wafa, W.M., 2021b. In vitro study on the potential fungicidal effects of atorvastatin in combination with some azole drugs against multidrug resistant Candida albicans. World J. Microbiol. Biotechnol. 37, 191. https://doi.org/10.1007/s11274-021-03158-4

Mahmoud, M.O., Aboud, H.M., Hassan, A.H., Ali, A.A., Johnston, T.P., 2017. Transdermal delivery of atorvastatin calcium from novel nanovesicular systems using polyethylene glycol fatty acid esters: Ameliorated effect without liver toxicity in poloxamer 407-induced hyperlipidemic rats. J. Control. Release 254, 10–22. https://doi.org/10.1016/j.jconrel.2017.03.039

Matusewicz, L., Meissner, J., Toporkiewicz, M., Sikorski, A.F., 2015. The effect of statins on cancer cells—review. Tumor Biol. 36, 4889–4904. https://doi.org/10.1007/s13277-015-3551-7

Mendyk, A., Jachowicz, R., Fijorek, K., Dorożyński, P., Kulinowski, P., Polak, S., 2012. KinetDS: An Open Source Software for Dissolution Test Data Analysis. Dissolution Technol. 19, 6–11. https://doi.org/10.14227/DT190112P6

Mirtič, J., Papathanasiou, F., Temova Rakuša, Ž., GosencaMatjaž, M., Roškar, R., Kristl, J., 2017. Development of medicated foams that combine incompatible hydrophilic and lipophilic drugs for psoriasis treatment. Int. J. Pharm. 524, 65–76. https://doi.org/10.1016/j.ijpharm.2017.03.061

Parsa, M., Trybala, A., Malik, D.J., Starov, V., 2019. Foam in pharmaceutical and medical applications. Curr. Opin. Colloid Interface Sci. 44, 153–167. https://doi.org/10.1016/j.cocis.2019.10.007

Peyclit, L., Yousfi, H., Rolain, J.-M., Bittar, F., 2021. Drug Repurposing in Medical Mycology: Identification of Compounds as Potential Antifungals to Overcome the Emergence of Multidrug-Resistant Fungi. Pharmaceuticals 14, 488. https://doi.org/10.3390/ph14050488

Pradhan, S., Hedberg, J., Blomberg, E., Wold, S., Odnevall Wallinder, I., 2016. Effect of sonication on particle dispersion, administered dose and metal release of non-

functionalized, non-inert metal nanoparticles. J. Nanoparticle Res. https://doi.org/10.1007/s11051-016-3597-5

Rayens, E., Norris, K.A., 2022. Prevalence and Healthcare Burden of Fungal Infections in the United States, 2018. Open Forum Infect. Dis. 9. https://doi.org/10.1093/ofid/ofab593

Rial, R., Hervas, L.S., Monux, G., Galindo, A., Martin, A., Hernando, M., Martinez, I., Hernando, A., Serrano, F.J., 2014. Polidocanol foam stability in terms of its association with glycerin. Phlebol. J. Venous Dis. 29, 304–309. https://doi.org/10.1177/0268355513477858

Sawant, D., Dandagi, P.M., Gadad, A.P., 2016. Formulation and evaluation of sparfloxacin emulsomes-loaded thermosensitive in situ gel for ophthalmic delivery. J. Sol-Gel Sci. Technol. 77, 654–665. https://doi.org/10.1007/s10971-015-3857-8

Senyiğit, Z.A., Karavana, S.Y., Eraç, B., Gürsel, O., Limoncu, M.H., Baloğlu, E., 2014. Evaluation of chitosan based vaginal bioadhesive gel formulations for antifungal drugs. Acta Pharm. 64, 139–56. https://doi.org/10.2478/acph-2014-0013

Shahraeini, S.S., Akbari, J., Saeedi, M., Morteza-Semnani, K., Abootorabi, S., Dehghanpoor, M., Rostamkalaei, S.S., Nokhodchi, A., 2020. Atorvastatin Solid Lipid Nanoparticles as a Promising Approach for Dermal Delivery and an Anti-inflammatory Agent. AAPS PharmSciTech 21, 263. https://doi.org/10.1208/s12249-020-01807-9

Song, F., Chen, J., Zheng, A., Tian, S., 2022. Effect of sterols on liposomes: Membrane characteristics and physicochemical changes during storage. LWT 164, 113558. https://doi.org/10.1016/j.lwt.2022.113558

Sousa, F., Ferreira, D., Reis, S., Costa, P., 2020. Current Insights on Antifungal Therapy: Novel Nanotechnology Approaches for Drug Delivery Systems and New Drugs from Natural Sources. Pharmaceuticals 13, 248. https://doi.org/10.3390/ph13090248

Sultana, J., Crisafulli, S., Gabbay, F., Lynn, E., Shakir, S., Trifirò, G., 2020. Challenges for Drug Repurposing in the COVID-19 Pandemic Era. Front. Pharmacol. 11, 1–13. https://doi.org/10.3389/fphar.2020.588654

Suvarna, S.K., Layton, C., Bancroft, J.D., 2012. Bancroft's Theory and practice of histological techniques, Seventh ed. ed. Elsevier Health Sciences.

Tamarkin, D., 2016. Foam: A Unique Delivery Vehicle for Topically Applied Formulations, in: Handbook of Formulating Dermal Applications. John Wiley & Sons, Inc., Hoboken, NJ, USA, pp. 233–260. https://doi.org/10.1002/9781119364221.ch9

Tavakkoli, A., Johnston, T.P., Sahebkar, A., 2020. Antifungal effects of statins. Pharmacol. Ther. 208, 107483. https://doi.org/10.1016/j.pharmthera.2020.107483

Varshosaz, J., Raghami, F., Rostami, M., Jahanian, A., 2019. PEGylated trimethylchitosan emulsomes conjugated to octreotide for targeted delivery of sorafenib to hepatocellular carcinoma cells of HepG2. J. Liposome Res. 29, 383–398. https://doi.org/10.1080/08982104.2019.1570250

Wang, H., Li, J., Wang, Z., Wang, D., Zhan, H., 2017. Experimental Investigation of the

Mechanism of Foaming Agent Concentration Affecting Foam Stability. J. Surfactants Deterg. 20, 1443–1451. https://doi.org/10.1007/s11743-017-2004-2

Wang, Y., Zhang, Y., Liu, Y., Zhang, L., Ren, S., Lu, J., Wang, X., Fan, N., 2017. The stability study of CO2 foams at high pressure and high temperature. J. Pet. Sci. Eng. 154, 234–243. https://doi.org/10.1016/j.petrol.2017.04.029

Woertz, J.R., Kinney, K.A., 2004. Influence of Sodium Dodecyl Sulfate and Tween 20 on Fungal Growth and Toluene Degradation in a Vapor-Phase Bioreactor. J. Environ. Eng. 130, 292–299. https://doi.org/10.1061/(ASCE)0733-9372(2004)130:3(292)

Yadav, M., Schiavone, N., Guzman-Aranguez, A., Giansanti, F., Papucci, L., Perez de Lara, M.J., Singh, M., Kaur, I.P., 2020. Atorvastatin-loaded solid lipid nanoparticles as eye drops: proposed treatment option for age-related macular degeneration (AMD). Drug Deliv. Transl. Res. 10, 919–944. https://doi.org/10.1007/s13346-020-00733-4

Zakaria, M.Y., Georghiou, P.E., Banoub, J.H., Beshay, B.Y., 2022. Inclusion of a Phytomedicinal Flavonoid in Biocompatible Surface-Modified Chylomicron Mimic Nanovesicles with Improved Oral Bioavailability and Virucidal Activity: Molecular Modeling and Pharmacodynamic Studies. Pharmaceutics 14, 905. https://doi.org/10.3390/pharmaceutics14050905

Zhang, L., Li, X., Zhu, S., Zhang, T., Maimaiti, A., Ding, M., Shi, S., 2020. Dermal Targeting Delivery of Terbinafine Hydrochloride Using Novel Multi-Ethosomes: A New Approach to Fungal Infection Treatment. Coatings 10, 304. https://doi.org/10.3390/coatings10040304

Zhang, X., Song, F., Taxipalati, M., Wei, W., Feng, F., 2014. Comparative Study of Surface-Active Properties and Antimicrobial Activities of Disaccharide Monoesters. PLoS One 9, e114845. https://doi.org/10.1371/journal.pone.0114845

Zhang, Y., Huo, M., Zhou, J., Zou, A., Li, W., Yao, C., Xie, S., 2010. DDSolver: An Add-In Program for Modeling and Comparison of Drug Dissolution Profiles. AAPS J. 12, 263–271. https://doi.org/10.1208/s12248-010-9185-1

Zhao, G.D., Sun, R., Ni, S.L., Xia, Q., 2015. Development and characterisation of a novel chitosan-coated antioxidant liposome containing both coenzyme Q10 and alpha-lipoic acid. J. Microencapsul. 32, 157–165. https://doi.org/10.3109/02652048.2014.973072

Zhao, Y., Brown, M.B., Jones, S.A., 2010a. The effects of particle properties on nanoparticle drug retention and release in dynamic minoxidil foams. Int. J. Pharm. 383, 277–284. https://doi.org/10.1016/j.ijpharm.2009.09.029

Zhao, Y., Jones, S.A., Brown, M.B., 2010b. Dynamic foams in topical drug delivery. J. Pharm. Pharmacol. 62, 678–84. https://doi.org/10.1211/jpp.62.06.0003

Zhou, X., Chen, Z., 2015. Preparation and performance evaluation of emulsomes as a drug delivery system for silybin. Arch. Pharm. Res. 38, 2193–2200. https://doi.org/10.1007/s12272-015-0630-7

Figures and Tables Captions

Scheme 1. Study design**:** *Phase 1* depicted the formulation and evaluation of atorvastatin-loaded emulsome (ATO-EMLs), *Phase 2* represents formulation and evaluation of blank foam systems, *Phase 3* shows further characterization of optimized ATO-EMLs foam system, *Phase 4* demonstrates skin tissue permeation by in-vivo visualization study using the confocal laser scanning microscope, *Phase 5* represents the microbiology studies of atorvastatin against C.albicans and A.fumigatus, *Phase 6* revealed the in-vivo studies.

Fig.1. 3D plot of cholesterol weight and sonication time impact as independent variables on (a) Particle size (PS), (b) Polydispersity index (PDI), (c) Zeta potential (ZP), and (d) Entrapment efficiency (EE), **Graphically illustrated of variables interaction** upon studying (e) Particle size (PS), (f) Polydispersity index (PDI), (g) Zeta potential (ZP), and (h) Entrapment efficiency (EE); results represent the significant influence of cholesterol on all variables, otherwise, sonication time affect PS and PDI only.

Fig.2. (a) **Interaction plot** showing independent variables desirability for selected ATO-EMLs optimum formula, **Further characterization on the optimum formula:** (b) TEM image of emulsome vesicle system; observed uniform spherical shape around 300 nm in size, (c) Fourier transforms infrared spectra for free atorvastatin, cholesterol, compritol, phosphatidylcholine, and optimum emulsome formula; prove vesicle formation and efficient drug loading.

Fig.3. 3D plots of foam expansion (%) response corresponding to different variable levels; **pluronic low level:** 0% (w/v) with different concentration (% w/v) of Tween 20 (a) 0, (b) 2, (c) 4, **pluronic medium level:** 2% (w/v) with different concentration (% w/v) of Tween 20 (d) 0, (e) 2, (f) 4, **pluronic high level:** 4% (w/v) with different concentration (% w/v) of Tween 20 (g) 0, (h) 2, (i) 4. (Measured response color change from blue to red indicate increase response value)

Fig.4. 3D plots of foam volume stability (%) response corresponding to different variable levels; **pluronic low level:** 0% (w/v) with different concentration (% w/v) of Tween 20 (a) 0, (b) 2, (c) 4, **pluronic medium level:** 2% (w/v) with different concentration (% w/v) of Tween 20 (d) 0, (e) 2, (f) 4, **pluronic high level:** 4% (w/v) with different concentration (% w/v) of Tween 20 (g) 0, (h) 2, (i) 4.

Fig.5. 3D plots of foam liquid stability (%) response corresponding to different variable levels; **pluronic low level:** 0% (w/v) with different concentration (% w/v) of Tween 20 (a) 0, (b) 2, (c) 4, **pluronic medium level:** 2% (w/v) with different concentration (% w/v) of Tween 20 (d) 0, (e) 2, (f) 4, **pluronic high level:** 4% (w/v) with different concentration (% w/v) of Tween 20 (g) 0, (h) 2, (i) 4.

Fig.6. 3D plots of half-life response corresponding to different variable levels; **pluronic low level:** 0% (w/v) with different concentration (% w/v) of Tween 20 (a) 0, (b) 2, (c) 4, **pluronic medium level:** 2% (w/v) with different concentration (% w/v) of Tween 20 (d) 0, (e) 2, (f) 4, **pluronic high level:** 4% (w/v) with different concentration (% w/v) of Tween 20 (g) 0, (h) 2, (i) 4.

Fig.7. 3D plots of viscosity response corresponding to different variable levels; **pluronic low level:** 0% (w/v) with different concentration (% w/v) of Tween 20 (a) 0, (b) 2, (c) 4, **pluronic medium level:** 2% (w/v) with different concentration (% w/v) of Tween 20 (d) 0, (e) 2, (f) 4, **pluronic high level:** 4% (w/v) with different concentration (% w/v) of Tween 20 (g) 0, (h) 2, (i) 4.

Fig.8. Design optimization model concerning variables and targeted responses; (a) desirability contour plot, (b) graphical optimization contour plot, **Comparative study** of ATO-EMLs foam with vesicle dispersion and blank foam regarding (c) Particle size, (d) Polydispersity index, (e) Foam calculated parameters, (f) and foam half-life; revealed insignificant differences as loaded foam conserve the optimum specifications.

Fig.9. (a) Depicted foam collapse time from the side view after activating; showing good stable structure with a long collapse time, (b) measured and analyzed bubble size and distribution using ImageJ software.

Fig. 10. (a) **Release study** illustrated as cumulative percentage of atorvastatin free drug in comparison to optimized ATO-EMLs before and after incorporation in foam system, **Stability study for 6 months**, evaluated sample storage at 4°C represented by (b) Particle size, (c), polydispersity index, and (d) Zeta potential; reflect stable attributes with no significant difference in comparison to fresh sample.

Fig. 11. Confocal laser scanning microscopy images of EMLs-foam system (a) tile x-y image of skin treated with FDA-loaded emulsome foam system, (b) 3D plot using z-stack images of the skin section from 0 µm to 300 µm with 15 µm increments, and (c) sequential images from 0-300 µm showed that penetration occurred across different skin layers revealed with high fluorescence intensity, (d) quantitative measurement of fluorescence intensity profile across skin layers.

Fig.12. *In-vitro* microbiology studies: In way to determine MIC; optical density values of two fungal species against the diluted concentration of the evaluated samples were determined (a) *C.albicans,* (b) *A.fumigatus,* the susceptibility of isolated fungal species to atorvastatin, blank and ATO-loaded EMLs foam in addition to commercial control was estimated through measured (c) MIC values, (d) diameters of inhibition zone, inhibition zones on C. albicans were visualized for (e) Atorvastatin, (f) ATO-EMLs foam, (g) blank-EML foam, (h) Commercial control, inhibition zones on *A.fumigatus* were visualized for (i) Atorvastatin, (j) ATO-EMLs foam, (k) Blank-EML foam, (l) Commercial control.

Fig.13. *In-vivo* biocompatibility study: (a) Normal skin, **(b)** placebo foam after 1 week, **(c)** placebo foam after 3 weeks, **(d)** ATO-EML foam after 1 week, **(e)** ATO-EMLs after 3 weeks.

Fig.14. *In-vivo* microbiological study: photographic images of the infected skin area of rat dorsal **(a)** positive control group, **(b)** standard drug group, and **(c)** ATO-EML foam group. **(d)** *C. Albicans* concentration in CFU/mL of different groups (**** $p < 0.0001$). Histopathological evaluation: **(e)** Positive group, **(f)** Standard drug group, **(g)** ATO-EML foam.

Graphical Abstract

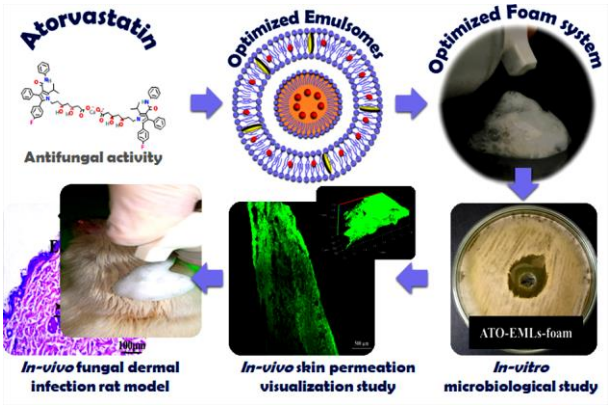

Author Contributions

Alaa S. Eita: methodology, data curation, formal analysis, investigation, writing-original draft, writing-review and editing, and visualization. **Amna M. A. Makky**: conceptualization, methodology, writing-original draft, writing-review and editing. **Asem Anter**: methodology, data curation, formal analysis, investigation. **Islam A. Khalil**: conceptualization, methodology, data curation, formal analysis, investigation, writing-original draft, writing-review and editing, visualization, funding acquisition, and project administration.

Declaration of interests

☒The authors declare that they have no known competing financial interests or personal relationships that could have appeared to influence the work reported in this paper.

☐The authors declare the following financial interests/personal relationships which may be considered as potential competing interests: